

DETECTING SPATIAL PATTERNS OF CHANGE IN VEGETATION INSIDE BAVARIAN FOREST NATIONAL PARK USING MULTI- AND HYPERSPECTRAL DATASETS

*Thesis submitted in partial fulfilment of the requirements for the degree of
Master of Science in Geoinformatics*



Internal Supervisor

Prof. Dr. Edzer Pebesma
Institute for Geoinformatics
University Of Münster

External Supervisors

Mrs. Stefanie Holzwarth & Dr. Martin Bachmann
Department Land Surface Dynamics
Agroecosystems and Phenology Team
Deutsches Zentrum für Luft- und Raumfahrt (DLR)

Submitted by

Nivedita Priyadarshini Kamaraj

Matriculation Number: 511868

28.03.2022

Declaration of Academic Integrity

I hereby confirm that this thesis on **Detecting spatial patterns of change in vegetation inside Bavarian Forest National Park using multi- and hyperspectral Datasets** is solely my own work and that I have used no sources or aids other than the ones stated. All passages in my thesis for which other sources, including electronic media, have been used, be it direct quotes or content references, have been acknowledged as such and the sources cited.

25.03.2022



(date and signature of student)

I agree to have my thesis checked in order to rule out potential similarities with other works and to have my thesis stored in a database for this purpose.

25.03.2022



(date and signature of student)

ACKNOWLEDGMENTS

I would like to extend my sincere thanks to my external thesis supervisors Mrs. Stefanie Holzwarth, Dr. Martin Bachmann from DLR, for their constant support and valuable guidance throughout this work. The completion of this study could not have been possible without their resourceful insights and timely suggestions.

I also extend my sincere gratitude to Prof. Dr. Edzer Pebesma from IFGI for providing valuable ideas, comments, and support in each phase of this research work.

I wish to share my gratitude to all the lecturers, course coordinators, and friends at IFGI.

A heartfelt thanks to my parents, brother, and grandparents, who have been motivating and supporting me since the first day of this project. Thanks for providing moral encouragement and having faith in me.

My special thanks to Nitheshnirmal for being alongside me constantly and helping me out during difficult times. I would also like to thank my friends Vinotha, Sindhu, and Rachael, who always encouraged me.

At last, I would like to thank the Almighty for giving me the strength and courage to complete this work!

ABSTRACT

Forests are an integral part of the natural ecosystem and are beneficial to humankind in many ways. Natural disturbances, both biotic (insects and pathogens) as well as abiotic (wildfire, drought, windthrow) are key processes in temperate forest ecosystems. Recent increases in both disturbance severity and frequency have been observed around the globe. Nowadays, numerous forest condition monitoring studies implementing remote sensing datasets for assessing biophysical and biochemical properties of vegetation species are widely used. The purpose of this study is to monitor changes in vegetation conditions inside the Bavarian Forest National Park (BFNP) which are mostly induced by outbreaks of the European Spruce Bark Beetle. For this purpose, a novel hyperspectral dataset acquired by the DLR Earth Sensing Imaging Spectrometer (DESI) along with Sentinel-2 Multispectral (S2 MSI) time series are used. This study aims to develop an integrated approach by examining spatial-temporal patterns and spectral properties using Vegetation Indices (VIs) to identify stressed conifers vegetation. Computation of several VIs enables to analyze the spatial patterns of change in vegetation happening inside the BFNP. The BFNP has a mixture of tree species, of which conifers are mainly affected by bark beetles. Seasonal variation in conifers from 2017 to 2021 are estimated for S2 MSI using a vegetation vitality index called Combined Vegetation Index (CVI). In addition, narrow-band indices are estimated for multi-annual DESI data between 2019 and 2021 to determine a suitable spectral index to identify changes in vegetation conditions. Results show CVI from S2 in combination with narrowband VI Modified Chlorophyll Absorption Ratio Index (MCARI) from DESI performs well in identifying changes due to infestation. Also, mean CVI from the S2 time-series shows subtle changes when observed season-wise. Finally, the results are validated in correspondence with in-situ field observations of bark beetle infested areas. Accuracies are acquired by validating the combined index results with ground truth data from which (i) area-based calculation provided initially 54% to improved accuracy of 63% when excluding smaller regions of infested areas, (ii) polygon-based yielded 57% mapped correctly increasing to 63% when focusing on larger pixels than DESI. The study also concludes that S2 results can be reliable if there is no imbalance in time series for each season. Also, DESI provides high-quality spectral input data suitable for mapping inter-annual changes in vegetation conditions.

Keywords: DESI, S2 MSI, Bavarian Forest National Park, bark beetle infestation, Narrowband VIs.

TABLE OF CONTENTS

1. Introduction	7
1.1. Motivation	7
1.2. Knowledge gap	8
1.3. Research questions	9
1.4. Research objectives	9
2. Materials and methods	10
2.1. Study area	10
2.2. Datasets	12
2.3. Methodology	13
2.3.1 Data quality assessment	14
2.3.2 Examining Spectral properties for DESIS and S2 MSI	15
2.3.3 Calculation of VIs for S2 MSI time series	19
2.3.4 Estimating annual change in vegetation using narrowband VIs for DESIS	20
2.3.5 Validation and accuracy assessment	21
3. Results	23
3.1 Seasonal changes from S2 CVI time series	23
3.2 Temporal change estimated from DESIS narrowband VIs	28
3.3 Threshold definition	38
3.4 Validation results	41
3.4.1 Product intercomparison	41
3.4.2 Analysis of combined detection Index	41
3.4.3 Accuracy assessment	45
3.4.3.1 Confusion matrix for raster in ENVI	45
3.4.3.2 Accuracies by matching vectors in QGIS	46
4. Discussion	49
5. Conclusion and recommendation	51
5.1. Conclusions	51
5.2. Recommendations	52
REFERENCES	53
APPENDICES	59

LIST OF FIGURES

Figure 1. Monthly precipitation observed in BFNP from January 2019 to December 2021	10
Figure 2. Study area location map	11
Figure 3. DESIS and S2 MSI datasets acquired over the BFNP between 2017 and 2021	13
Figure 4. Formulated workflow	14
Figure 5. Mean spectra of DESIS with conifers/deciduous/mixed species for 2019	16
Figure 6. Mean spectra of DESIS with conifers/deciduous/mixed species for 2021	16
Figure 7. Mean spectra assessed for conifers between 2019 and 2021 for DESIS	17
Figure 8. Interactive Red Edge Inflection Point from EnMAP toolbox	17
Figure 9. Mean spectral plots of S2 MSI for (a) Fall, (b) Spring and (c) Summer from 2017 - 2021....	18
Figure 10. Mean CVI mapped for S2 MSI season wise.....	25
Figure 11. Comparison of S2 NDRE index between Conifers vs stressed conifers.....	26
Figure 12. Comparison of S2 NDVI index between Conifers vs stressed conifers.	26
Figure 13. Comparison of S2 VIGreen index between Conifers vs stressed conifers.	27
Figure 14. Comparison of S2 mean CVI values between Conifers vs stressed conifers.....	27
Figure 15. Temporal change calculated for PSRI for DESIS between 2019 and 2021	30
Figure 16. Temporal change calculated for PRI for DESIS between 2019 and 2021	31
Figure 17. Temporal change calculated for MRESR for DESIS between 2019 and 2021	31
Figure 18. Temporal change calculated for GI for DESIS between 2019 and 2021	32
Figure 19. Temporal change calculated for SR for DESIS between 2019 and 2021	32
Figure 20. Temporal change calculated for ARI for DESIS between 2019 and 2021	33
Figure 21. Temporal change calculated for CRI- 1 for DESIS between 2019 and 2021.....	33
Figure 22. Temporal change calculated for CRI-2 for DESIS between 2019 and 2021.....	34
Figure 23. Temporal change calculated for VREI for DESIS between 2019 and 2021.....	34
Figure 24. Temporal change calculated for REP for DESIS between 2019 and 2021.....	35
Figure 25. Temporal change calculated for MRENDVI for DESIS between 2019 and 2021	35
Figure 26. Temporal change calculated for MCARI for DESIS between 2019 and 2021	36
Figure 27. Temporal change calculated for NDRE for DESIS between 2019 and 2021	37
Figure 28. Temporal change calculated for NDVI for DESIS between 2019 and 2021	37
Figure 29. MCARI negative changes matching with orthomosaics and ground truth reference data with ≤ -0.005 threshold.....	39
Figure 30. CVI negative changes matching with ground truth polygons with ≤ -0.35 threshold.	40
Figure 31. Changes detected using Combined detection index from both DESIS and S2 indices with modified thresholds.....	44
Figure 32. Changes detected validated using orthomosaic and ground truth polygons	45

LIST OF TABLES

Table 1. Characteristics of datasets used	12
Table 2. CVI calculated from VIs for S2 MSI	20
Table 3. Narrowband VIs for DESIS	21
Table 4. JD labeled for S2 MSI time series.....	23
Table 5. Narrowband indices for temporal change estimation using DESIS	28
Table 6. Logic for the Combined detection index “MCARI – CVI”	42
Table 7. Logic for modified Combined detection index “2*MCARI + CVI”	42
Table 8. Overall accuracies of percent change and no change compared between original, buffer and clump classes for MCARI and CVI	46
Table 9. Accuracies with respect to area coverage	47
Table 10. Accuracies with respect to number of polygons	48
Table 11. Accuracies based on polygon count with varied pixel size	48

1. INTRODUCTION

1.1. Motivation

Forests are an important part of the natural environment which spreads nearly over 30% of the earth's surface [1,2]. The ecosystem services and socio-economic benefits provided by forests are immense to the mankind [3–6]. Apart from which, forests also provide resistance against erosion and help in controlling the flood. Even though the forests were exploited for centuries, people in recent times started recognizing the need for the existence and good health of the forests. Forest health is often naturally disturbed by both biotic and abiotic agents [7]. In addition, global changes such as human influenced climate change increases the effect of both biotic and abiotic agents in degrading the forest health in unprecedented ways [1,8–10]. Globally in recent times, there has been an upsurge in the occurrence of disturbance events [11,12]. Furthermore, forecast models also predict that there will be an increase in the number of disturbance events in the coming years which would largely affect the forest health [13–15]. Increasing disturbance events can result in significant loss in the ecosystem services and benefits obtained from forests[9,16]. Given the significance of the forests and the threat to their health, forest health monitoring is a requisite for the implementation of sustainable management of forests [17–21].

Most forests in Central Europe have hilly or mountainous terrain with a densely wooded mixed variety of tree species showing diversity in growth and other phenological aspects. Apparent changes in individual species in climate-sensitive zones depend on altitude levels [22]. It was also a prominent fact observed in Central European forests that there was an annual change in vegetation seasonally, mainly with the proliferation of bark beetle (*Ips typographus*, L.) infestation which caused huge ecological loss by damaging vast spruce species [19,20,23,24]. The infestation was more obvious in all species of conifers when compared to that of deciduous forest types.

There have been both customary and modern methods used for monitoring the forest health. The traditional techniques, including inventory plotting through field surveying can be both time consuming and laborious [3]. In addition, traditional surveys can be only carried out annually due to its labor-intensive and time taking process. Furthermore, field surveys are suitable in the case of small areas whereas for covering a large area wouldn't be apt [25]. On the contrary, contemporary remote sensing techniques can aid in monitoring the health of forests over large areas easily [18,26–28]. Apart from covering large areas, remote sensing

helps in quick, repeatable, synoptic, and cost-effective monitoring of forest health [29]. For forest health monitoring using remote sensing, various bio-physical and bio-chemical indices are used by the researchers [17,18].

Timely monitoring of vegetation species and understanding their adaptability to external ecological factors are an integral part in preserving a healthy forest ecosystem [30]. Phenological changes in species observed on a larger scale is mainly due to climatological aspects. Each individual species undergo a shift based on climate fluctuations showing transition in distribution patterns [31]. Observing satellite imageries with longer time series provides in-depth records of changes happening within forest landscapes.

Hyperspectral sensors having several contiguous, narrow spectral bands serves a variety of vegetation mapping applications including forest health monitoring [32,33]. In recent times, there has been a greater utility of hyperspectral sensors due to its growing value in terms of accuracy compared to multispectral data [34]. Spectral bands of spaceborne and airborne hyperspectral remote sensing have unlocked approaches in agricultural and forest research especially in monitoring forest health assessment and its management [35,36]. One such novel hyperspectral dataset used for this study purpose is the DLR Earth Sensing Imaging Spectrometer (DESI) installed on the International Space Station (ISS), and jointly operated with Teledyne Brown Engineering in the USA. The hyperspectral instrument measures in the spectral range from 400 and 1000 nm with a spectral sampling distance of 2.55 nm [37]. DESI delivers accurate spectral measurements in a moderate spatial resolution of 30 m which can be useful in spatio-temporal measurement of the vegetation parameters over a wider area [38].

1.2. Knowledge gap

DESI, being a novel hyperspectral spaceborne data having higher spectral resolution, is compared with Sentinel-2 Multispectral Image data (S2 MSI), having finer spatial resolution, for evaluating the potentials to use both sensors in combination for monitoring the forest health. This study aims to develop an integrated approach by assessing spatio-temporal patterns by examining Vegetation Indices (VIs) to identify vegetation changes occurring in the forest. The study purely uses spaceborne remote sensor datasets to observe spatial patterns of vegetation change through VIs and the results are validated with ground truth samples from field observations. Computation of several VIs enable to analyze the spatial pattern of change in vegetation especially season-wise inside the BFNP. Additionally, pure

reflectance spectra extracted from spectral imagery discriminates between healthy vs. stressed vegetation. Moreover, the novelty of this study in specific is to compare and analyze synergies between multi-annual hyperspectral DESIS, multi-temporal S2 MSI time series through a variety of spectral indices to detect changes in vegetation happening inside the forest.

1.3. Research questions

A detailed analysis on the relationship between the higher spectral resolution of DESIS and S2 data, their different temporal and spatial resolution, and the resulting possibilities to use both systems in combination for monitoring tasks in the field of forest health are exploited. Implementing these datasets, the following research questions are examined which includes:

- What are the spatial patterns of vegetation change when analyzing time series and when focusing on spectral information?
- Do all narrowband indices of DESIS show similar temporal variations compared to multispectral time series, and which VIs and bio-physical indicators are most suitable?
- Do these patterns match with bark beetle-infested regions collected from the field?

1.4. Research objectives

The study aims to monitor forest health and detect spatial patterns of change in vegetation inside Bavarian Forest National Park (BFNP) using spaceborne hyperspectral and multispectral datasets. The objectives used for achieving the aim includes:

- To estimate seasonal variation in vegetation from 2017 to 2021 for S2 using Combined Vegetation Index (CVI) time series.
- To examine multi-annual DESIS data using narrowband VIs to determine the suitable spectral index.
- To analyze possibilities and limitations of DESIS data in comparison to and in combination with S2 data to serve this application.
- To validate the acquired results using additional information such as ground truth samples and high-resolution orthomosaics provided by BFNP team.

These objectives are fulfilled by incorporating a formulated workflow that is sub-divided into data preparation and preprocessing, analysis of indices and validation of results. This work was conducted in frame of the Data Pool Initiative for the Bohemian Forest Ecosystem [39].

2. MATERIALS AND METHODS

2.1. Study area

The study area opted is the BFNP in Germany. The BFNP covers a total area of 24,250 hectares bordering Czech Republic in the southeastern part of Germany. It has an altitude ranging from 600 to 1453 m above sea level. It has a mean annual temperature ranging between 2,0 – 5,0°C at high elevation regions and 3,0 – 6,5° C at the valley. The annual precipitation ranges between 830 – 2,280 mm at higher altitudes and 1,030 - 1,630 mm at valleys. It was also inferred from weather statistics of BFNP that, 2019 had 350 mm lower precipitation than average being recorded as the hottest year, and 2020 was the year with fewer snowy days exhibiting observable climate changes in the forest [40]. The graphs below in Figure 1 show monthly precipitation observed in BFNP from January 2019 to December 2021. The study location map is shown in Figure 2.

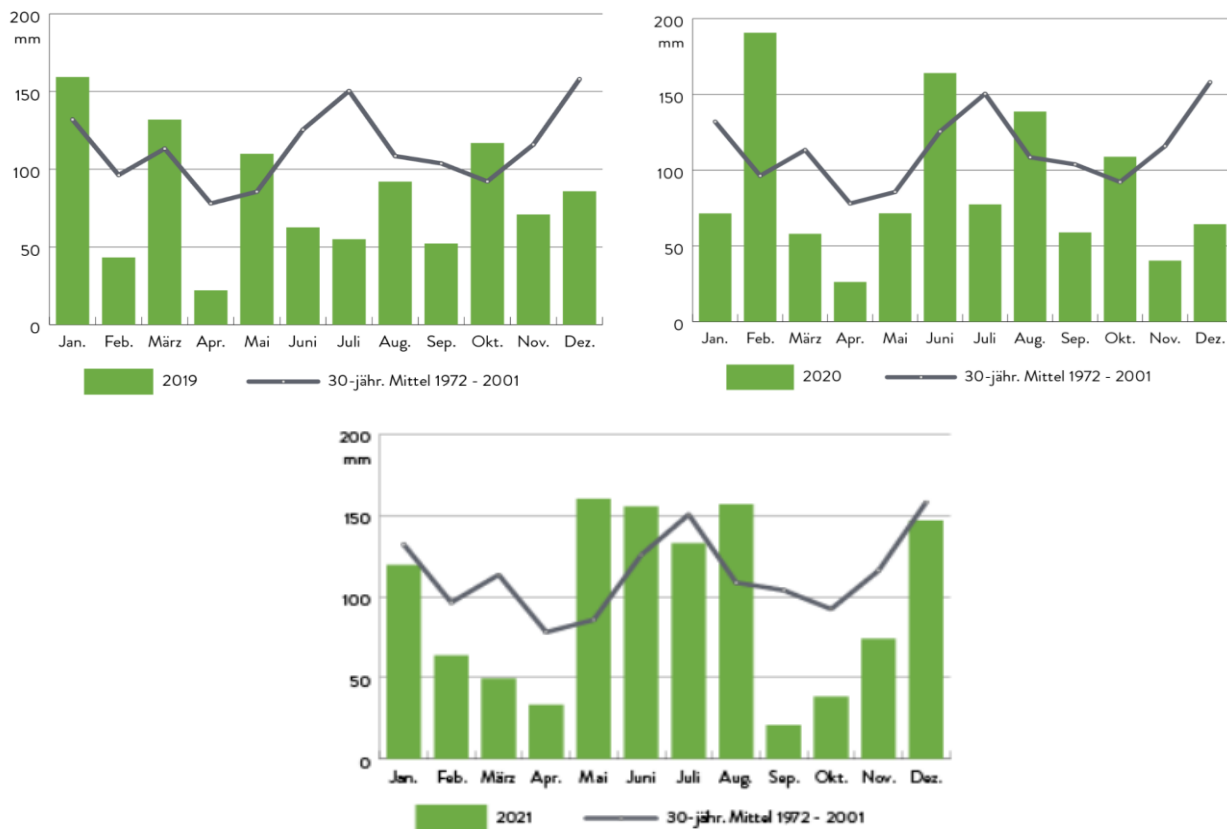


Figure 1. Monthly precipitation observed in BFNP from January 2019 to December 2021

The Park was established in the year 1970, and this forest ecosystem has about 70% of spruce conifer [41]. Some of the species identified are Norway spruce (*Picea abies* L.),

Mountain ash (*Sorbus aucuparia* L.) and Sycamore maple (*Acer pseudoplatanus* L.) [42]. Apart from these, the forest has a significant amount of deciduous and mixed tree species like silver fir (*Abies alba*) and European beech (*Fagus sylvatica*). In the National Park, it is seen during spring that when there is an increase in ambient air temperature, there occurs a notable damage caused by the bark beetles since 1990's [43]. The European spruce bark beetle are considered to be a dominant infestation outbreak showing distinct stress symptoms in healthy canopies. This attack in turn, causes change in needle color followed by shedding of needles leaving only grey bark remains. These are categorized to be dead trees or deadwood found inside the National Park [44]. These information can be gained with little or no human interference norms as per the policy of BFNP [42].

In this master thesis importance is given to the conifers species since changes are clearly visible due to any external environmental factors and they are mainly infested by the bark beetles. Also, conifers specifically show no phenological or seasonal changes like deciduous or mixed which tend to lose leaves every season.

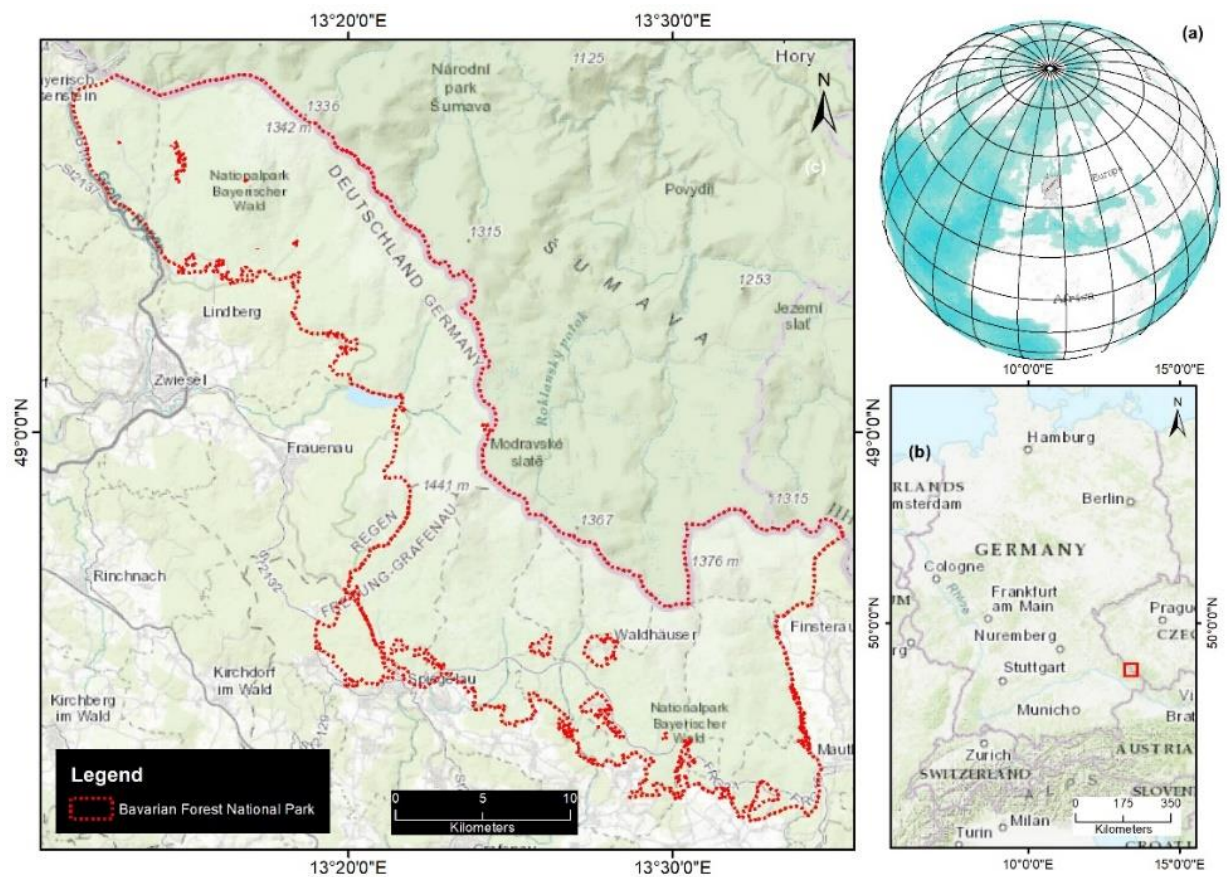


Figure 2. Study area location map

2.2. Datasets

The datasets used for the study includes hyperspectral DESIS Level-2A (L2A) products processed with DLR's processing chain [45] along with S2 MSI L2A time series datasets based on the MAJA processor [46]. The DESIS instrument is mounted at the International Space Station (ISS) and integrated through the Multi-User-System for Earth Sensing (MUSES) platform [38,47]. DESIS has a target lifetime from 2018 – 2023 and has a capacity to acquire data for about 3000 Km on ground. It is operated in an image strip acquisition mode rendering target-specific multi-angular characteristics with an off-nadir look angle of $\pm 15^\circ$ [38]. Some additional features about the datasets utilized are mentioned in Table 1.

Table 1. Characteristics of datasets used

DESIS L2A Product	S2 MSI L2A Product
<ul style="list-style-type: none"> • 4* binning with 60 Spectral bands (54 bands considered for analysis) at ~10.20 nm FWHM • Spatial resolution: 30 meters • Wavelength range: 400 to 1000 nm • Revisit frequency: 3 to 5 days (on an average) • Swath: 400 Km 	<ul style="list-style-type: none"> • 12 Spectral bands (9 bands considered for analysis) • Spatial resolution: 20 meters (for all bands, resampled) • Wavelength range: 490 to 2185 nm • Revisit time: 5 to 10 days • Swath: 290 Km

Some salient features of DESIS are it has a Pointing Unit (POI) with a rotating mirror having $\pm 15^\circ$ forward or backward change in view angle providing BRDF (Bidirectional Reflectance Distribution Function) measurements of targets in ground [47]. The instrument is also equipped with an in-built calibration and Inertial Measurement Unit (IMU). Initially, DESIS acquisitions over the BFNP started from 2019 with varied time, date of acquisitions and pointing angles. It had very few cloud-free footprints having acceptable quality rating. Since the ISS orbit is changing, DESIS does not have a fixed revisit time. Hence only a total of 10 cloud-free acquisitions starting from 12.06.2019 to 17.06.2021 were considered for analysis.

Additionally, to monitor seasonal changes in phenology of conifers over time, S2 MSI time series were considered. S2 MSI instrument uses three mirror telescopes operated at both Visible and Near-Infrared (VNIR) and Short-Wave Infrared (SWIR) wavelengths. This provides finer L2A Bottom-Of-Atmosphere (BOA) reflectance corrected products for both S2A and S2B utilized in this study. Positioning the two S2 sensors are maintained by a Global

Navigation Satellite System (GNSS) receiver. Sensors are equipped with an onboard diffuser for radiometric calibration [48]. Total of 20 S2 acquisitions from 13.07.2017 to 17.06.2021 were considered for this study. Processing these S2 tiles is useful to look at the changes in trend of vegetation with respect to season. DESIS and S2 time series acquisitions available for the study area are shown in Figure 3 below.

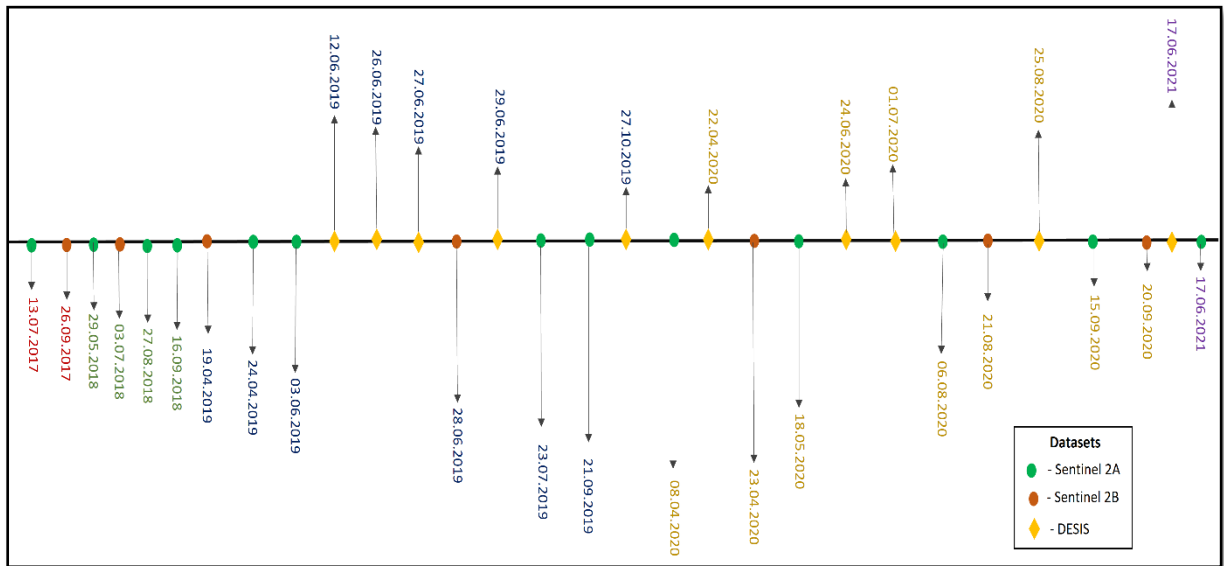


Figure 3. DESIS and S2 MSI datasets acquired over the BFNP between 2017 and 2021

2.3. Methodology

The methodology implemented for the study is represented in Figure 4. The workflow is split up into three parts namely preprocessing, indices analysis and validation for clear understanding.

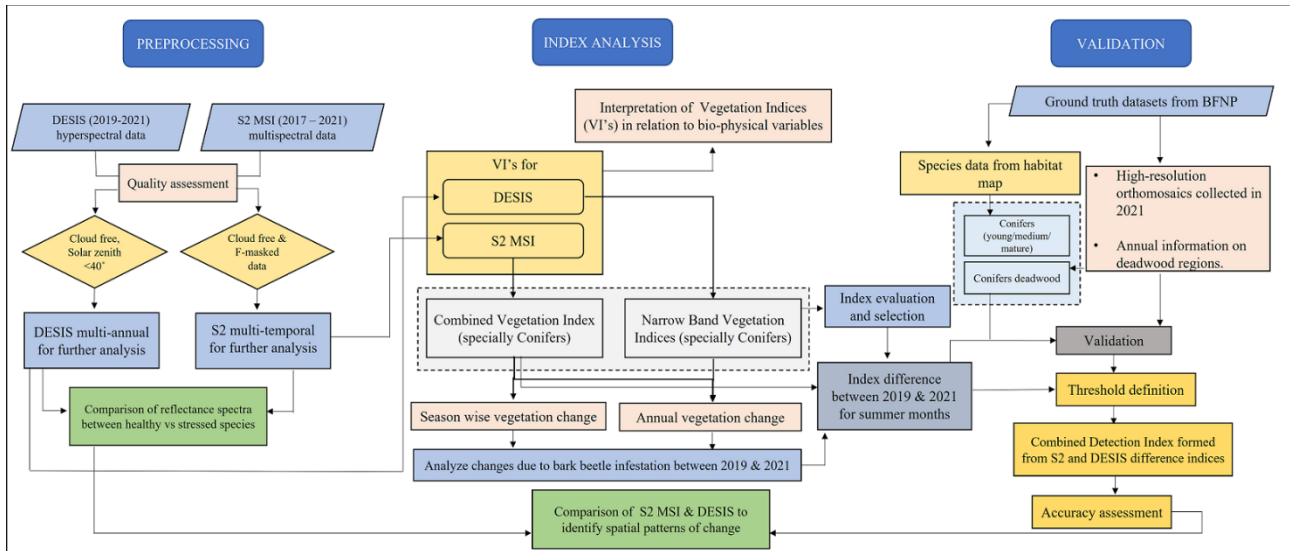


Figure 4. Formulated workflow

2.3.1 Data quality assessment

For the choice of optimal DESIS data from a series of several cloud-free available datasets a few factors were considered to be essential. L2A reflectance product with cloud-free acquisitions and solar zenith angle $<40^\circ$ that reduces shadows, effects in BRDF, influence of atmosphere and influence of anisotropic effects were selected. Two multi-annual DESIS datasets, 29.06.2019 and 17.06.2021 both from summer months were opted for detecting temporal changes in vegetation. As 2018 was the year with a larger infestation rate followed by 2019, one of the most drought-prone years of BFNP, the datasets from 2019 were well suited for assessing forest changes. Initially, with no spectral binning, there are 235 spectral bands in DESIS but for this study, 4xbinning with 60 spectral bands were selected as spectral resolution depends on bands. Bands 1-3 and 58-60 were removed to minimize any spectral distortions in the image. After removal of noisy bands, 54 spectral bands from 430-975 nm were considered for further processing.

A total of 20 multi-temporal S2 MSI time series were taken into account. In order to increase the number of datasets for the study, few tiles with some clouds were considered as well. These needed to be cloud masked using the F-mask algorithm [49,50]. About 9 spectral bands with ground reflectance corrected for slope effects for each S2 MSI scene from the MAJA processor were stacked for analysis [46].

2.3.2 Examining Spectral properties for DESIS and S2 MSI

Spectral reflectance for both datasets were observed for conifers which discriminates healthy vs. stressed vegetation. In DESIS, the spectral response from numerous pixels were collected and averaged as shown in Figure 5 for 2019 and Figure 6 for 2021 to obtain the mean spectra for different species type inside BFNP. Spectral signatures for conifers were observed closely around the infested zones which clearly shows a transition in curve. This type of transition shown in the stressed vegetation is so called “blue-shift” observed near the red-edge range of the spectrum [51,52]. It determines a reduction in green and NIR reflectance denoting green leaves under stress and for DESIS inflection is significant around 723nm, as shown in Figures 7 and 8. To detect the change in reflectance pattern a tool from the EnMAP toolbox known as Interactive Red Edge Inflection Point (iREIP) was used. The shift in patterns indicate vegetation stress that might have caused between 2019 – 2021 that are later examined in results of narrowband VIs. Mean reflectance spectra of stressed patches defines the traits such as cuticle, outer epidermal layer of the conifers and upper needle surface that are prone to infestation[53]. Like DESIS, the spectral response patterns from S2 MSI having better Ground Sampling Distance (GSD) yet coarser spectral resolution were analyzed for three seasons. For the entire S2, time-series mean reflectance spectra were generated as shown in Figure 9 for better understanding seasonal variations [54,55]. Pure crown spectra from S2 show few discrepancies which can be due to presence of cloud shadows or other outliers.

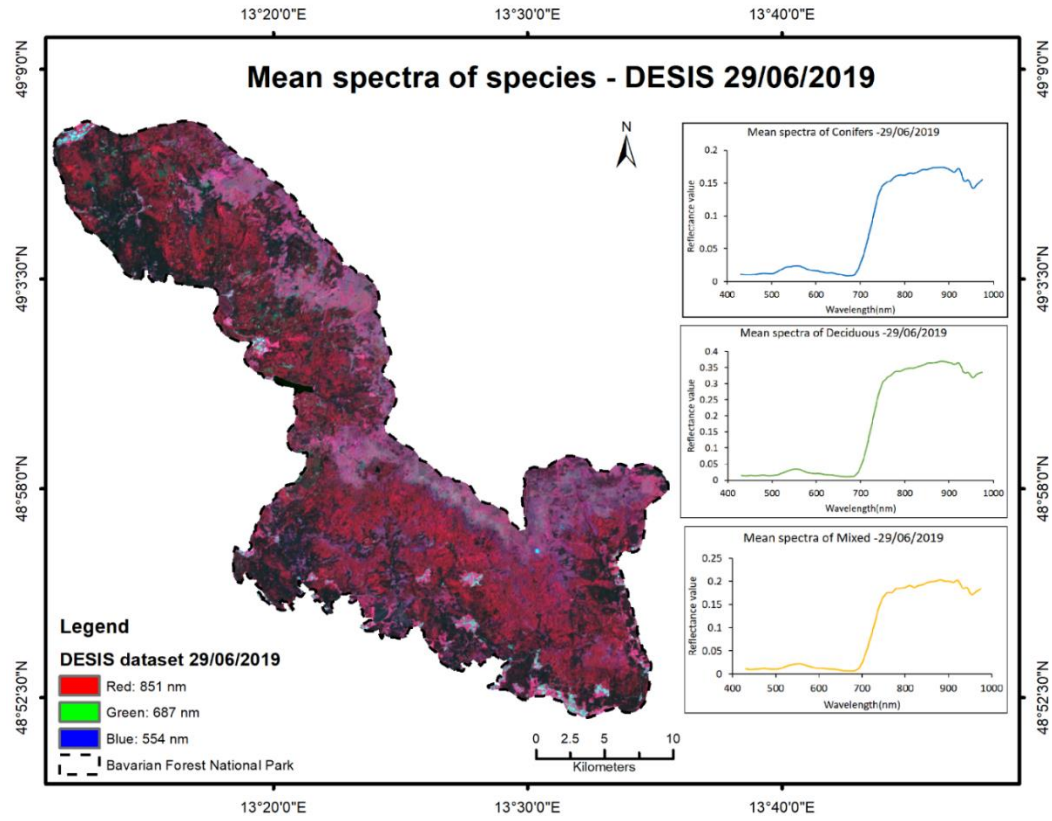


Figure 5. Mean spectra of DESIS with conifers/deciduous/mixed species for 2019

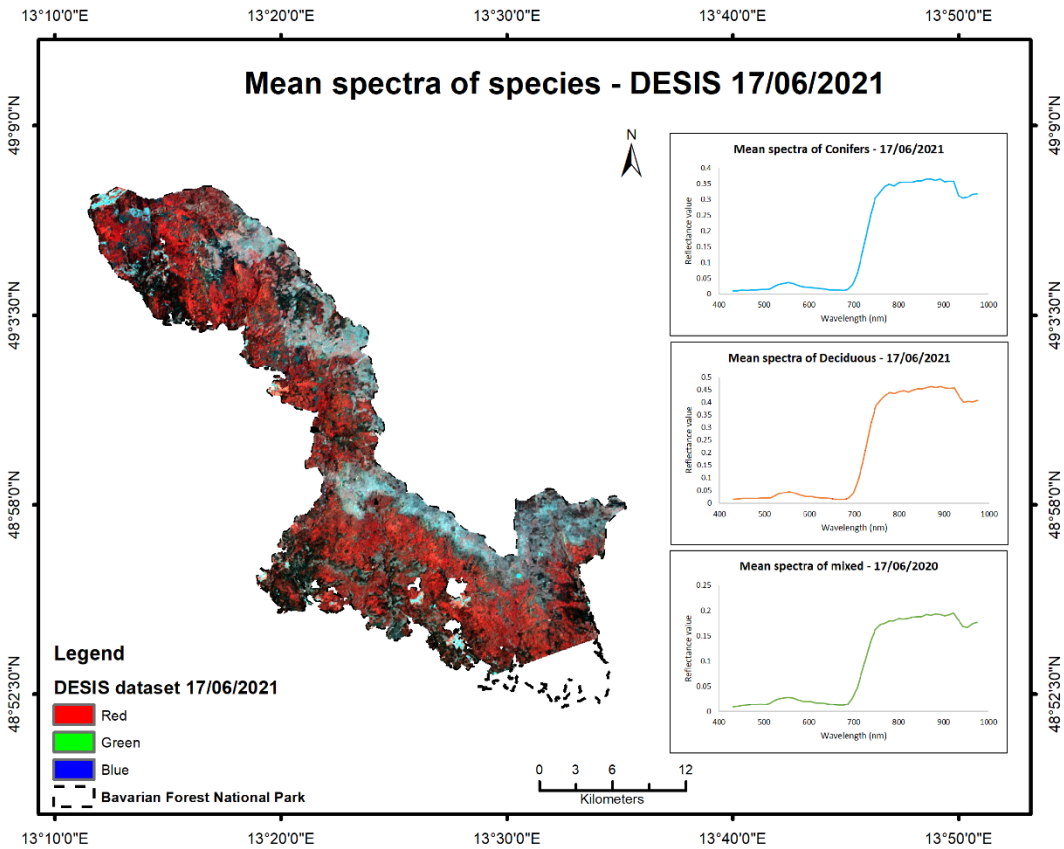


Figure 6. Mean spectra of DESIS with conifers/deciduous/mixed species for 2021

From the mean spectral plots of DESIS, conifers plots were checked for change in spectral pattern that denotes blue-shift near the red-edge to indicate stress in vegetation. On a closer observation as shown in Figure 7 the mean spectra plots clearly represents a shift in spectral response pattern which is also verified using the iREIP tool as shown in Figure 8.

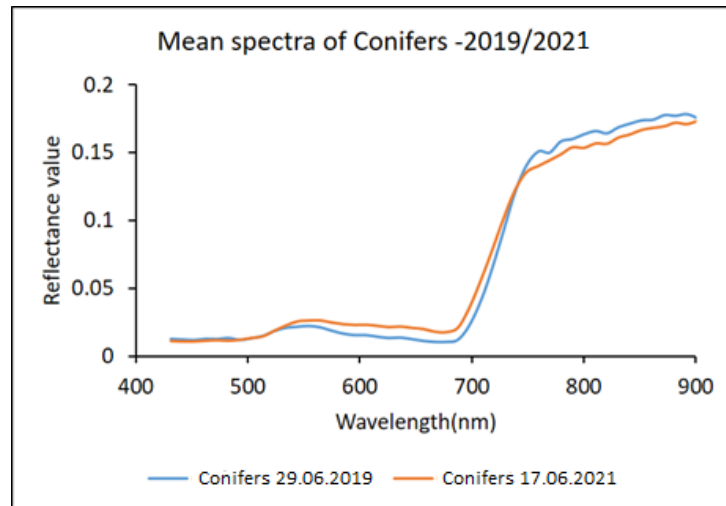


Figure 7. Mean spectra assessed for conifers between 2019 and 2021 for DESIS



Figure 8. Interactive Red Edge Inflection Point from EnMAP toolbox

Additionally, the spectral plots of S2 time series are assessed season wise which shows slight variations. Few plots such as 29.05.2018 in the spring and 03.07.2018 in summer are seen with greater variation which could be due to masking or not fully removed clouds. Plots for fall, spring and summer are shown in Figures 9.

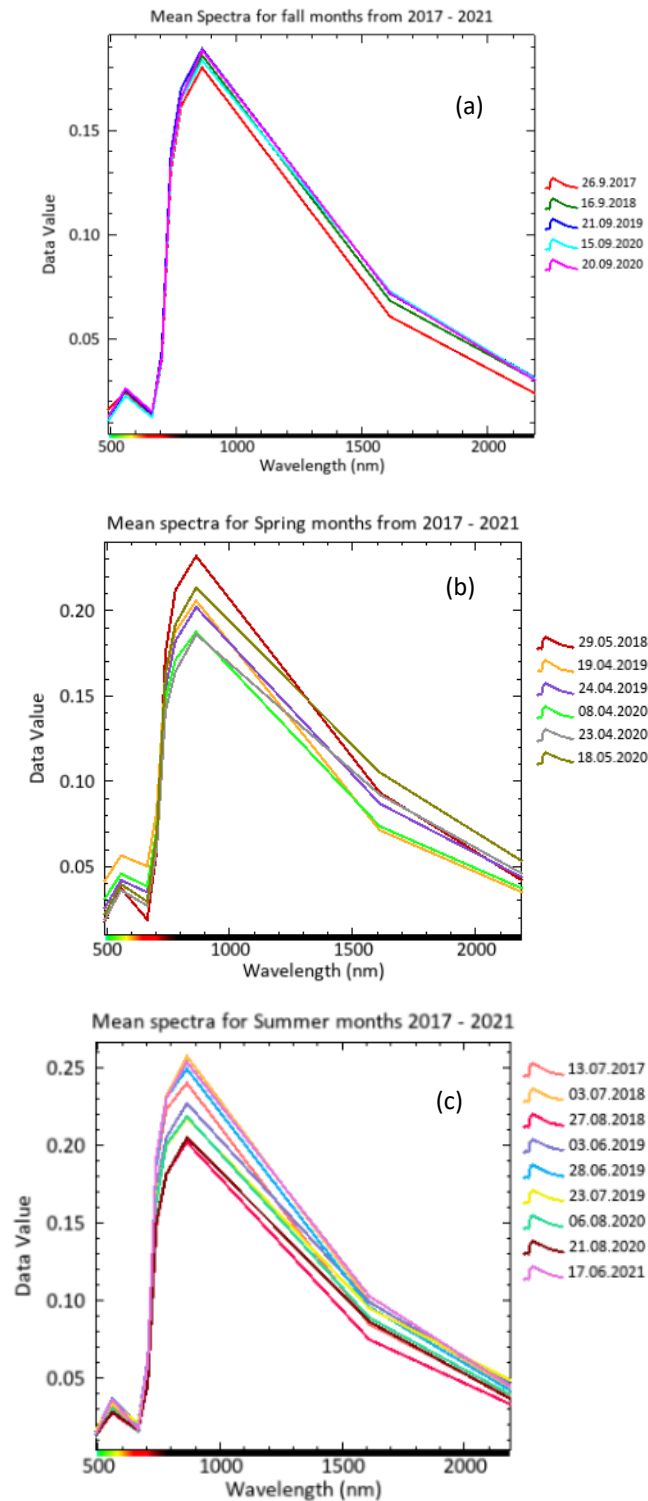


Figure 9. Mean spectral plots of S2 MSI for (a) Fall, (b) Spring and (c) Summer from 2017 - 2021

2.3.3 Calculation of VIs for S2 MSI time series

S2 MSI sensor renders high spatial data spectrally covering the VNIR-SWIR region with which a wide variety of VIs are calculated to identify changes in canopy properties. It was also inferred that S2 derived indices for detecting changes caused by bark beetle infestation showed improved results when compared to Landsat 8 datasets [56]. For this study, mostly cloud-free S2 MAJA corrected tiles were downloaded from 2017 to 2021. Compared to DESIS that has multi-annual datasets from 2019 and 2021, details from past forest events were required for better understanding the activities occurred at BFNP. Therefore, the time series of S2 were planned to be expanded from 2017. From the entire time-series of S2, a very few scenes from 2017 and 2018 namely on 26.09.2017 and 03.07.2018 were taken with cloud cover <20% as the cloud-free datasets were scarcely available for those years. A F-mask algorithm potential enough to mask out cloud and cloud shadows through object-based matching technique for each individual scene was applied using ENVI [49].

Forest phenology varies with disturbance events like bark beetle attack observed in conifers. However, with the time series years considered for this study and reports from authorities at BFNP it was understood that there was an infestation started to swarm during May 2016 [41] followed by another attack in early January 2018 with continued drought [57]. S2 MSI MAJA corrected tiles for BFNP were available only from 2017 with minimal cloud coverage and therefore multi-temporal images were categorized showing different periods based on seasonality. In general, the forest dynamic phase is ordered based on season, such as (1) spring months where new leaves are developed, followed by (2) summer months showing intense foliage coverage and finally (3) fall months that shows autumnal foliage.

A list of vegetation indices was estimated by considering the bio-physical variables such as structure, chlorophyll, and leaf pigment into account as VIs are specifically not always sensitive to a single variable. Utmost care is taken while choosing each index from bio-physical variable when concerned with heterogeneous canopy covers including healthy vs. stressed trees [58]. Estimation of vegetation indices are a prime component in analyzing forest health. Response from the vegetation indices can be used to quantify several exterior parameters like damage due to bark beetle infestation, drought, and wild forest fires that occur [17,59,60]. Since the entire forest health cannot be determined from a single vegetation index, a vegetation vitality index called CVI in Table 2, is proposed [61] by giving equal weightage to one index from every bio-physical variable. CVI is represented in equation 1 as:

$$CVI = \sum_{k=1}^n \text{One index per bio – physical property}_k / n \quad (1)$$

Table 2. CVI calculated from VIs for S2 MSI

Bio-physical variable	Index	Sentinel-2	DESIS (Wavelength in nm)
Structural component, LAI coverage	NDVI	$(\text{NIR} - \text{Red}) / (\text{NIR} + \text{Red})$	$(\rho_{\lambda 840} - \rho_{\lambda 666}) / (\rho_{\lambda 840} + \rho_{\lambda 666})$
Chlorophyll	NDRE	$(\text{NIR} - \text{RE}) / (\text{NIR} + \text{RE})$	$(\rho_{\lambda 779} - \rho_{\lambda 708}) / (\rho_{\lambda 779} + \rho_{\lambda 708})$
Leaf pigment	VI _{Green}	$(\text{Green} - \text{Red}) / (\text{Green} + \text{Red})$	$(\rho_{\lambda 554} - \rho_{\lambda 666}) / (\rho_{\lambda 554} + \rho_{\lambda 666})$
	CVI	$(\text{NDVI} + \text{NDRE} + \text{VI}_{\text{Green}}) / 3$	

2.3.4 Estimating annual change in vegetation using narrowband VIs for DESIS

It is stated that hyperspectral sensor imageries facilitate identifying forest disturbances by analyzing several narrowband VIs [62]. DESIS having contiguous narrow bands, increases the SNR providing capability to assess plant bio-physical parameters to explore forest health status. It provides in-depth spectral information in the visible, near infrared and red edge regions [63]. Besides, stress conditions in vegetation species are mapped using hyperspectral derivative reflectance especially by examining the red-edge range [64]. Varied traits in foliage cover such as LAI, chlorophyll content, or leaf nitrogen content are mapped by analyzing field spectra or other potentially derived VIs from high-quality airborne HySpex or other hyperspectral datasets taken over BFNP study site [55,65–67]. To fulfil this study objectives, for the multi-annual reflectance corrected DESIS summer month datasets, fourteen narrowband VIs were estimated and categorized based on bio-physical properties. The less frequent DESIS data is applied to emphasize the annual changes of forest condition in a more detailed manner. Regarding vegetation health, the bark beetle infested areas, in particular, were examined more closely. From the retrieved VI results, areas showing negative change in vegetation were checked for correspondence with the infested area field information provided. The narrowband VIs were estimated to quantify the temporal changes among conifers between 2019 and 2021. The narrowband VIs applied for DESIS are listed in Table 3. The indices are classified based on structural, chlorophyll, and other leaf-pigment properties defined to find the suitable index that enhances quality of spectrally precise input DESIS dataset. The results, in turn would reflect visible stressed conifers stands for which spectral properties can be checked and cross verified with geolocations of affected regions.

Table 3. Narrowband VIs for DESIS

Narrowband VI	Specific formula	Application/ Biophysical Property	Reference
Plant Senescence Reflectance Index	$PSRI = (678nm - 500nm) / 750 nm$	Dry or Senescent Carbon (Scale: Leaf)	[68]
Photochemical Reflectance Index	$PRI = (531nm - 570nm) / (531nm + 570nm)$	Chlorophyll	[69]
Modified Red Edge Simple Ratio	$MRESR = (750nm - 445nm) / (705 nm - 445nm)$	Chlorophyll	[70,71]
Greenness Index	$GI = 554nm / 677 nm$	Chlorophyll	[72]
Simple Ratio	$SR = 675nm / 700nm$	Chlorophyll	[73,74]
Anthocyanin Reflectance Index 1	$ARI1 = (1/550 nm - 1/700 nm)$	Leaf pigment	[75]
Carotenoid Reflectance Index 1	$CRI1 = (1/510 nm - 1/550 nm)$	Leaf pigment	[76]
Carotenoid Reflectance Index 2	$CRI2 = (1/510 nm - 1/700 nm)$	Leaf pigment	[76]
Vogelmann Red Edge Index 1	$VREI1 = (740nm / 720 nm)$	Chlorophyll	[77]
Red Edge Position Index	$REPI = 700 + 40 * ((670nm + 780nm / 2) - 700nm) / (740nm - 700nm)$	Chlorophyll	[78–80]
Modified Red Edge NDVI	$MRENDVI = (750 nm - 705 nm) / (750 nm + 705 nm - 2 * 445 nm)$	Chlorophyll	[71]
Modified Chlorophyll Absorption Ratio Index	$MCARI = [(700 nm - 670 nm) - 0.2(700 nm - 550 nm)] * (700 nm / 670nm)$	Chlorophyll	[81]
Normalized Difference Red Edge Index	$NDRE = (790nm - 720nm) / (790nm + 720nm)$	Chlorophyll	[82]
Normalized Difference Vegetation Index	$NDVI = (NIR - Red) / (NIR + Red)$	Structure	[83]

2.3.5 Validation and accuracy assessment

It is essential to examine the correctness of classes with respect to reference data that emphasizes the usage of remote sensing imageries. An overall accuracy exhibits pixels correctly classified or misclassified that defines the reliability of processing [84]. From the confusion matrix, dividing the sum of correctly classified values with total number of ground truth values provides an overall accuracy which is a measure of performance and a kappa

value which is a measure of agreement between change class vs ground truth reference [85–87]. In this study, retrieved results are validated using in-situ observations collected from the BFNP. Ground truth datasets used for validation includes shapefile information of infested regions, mainly due to bark beetles from 2019 – 2021 and an airborne orthomosaics collected between 14.06.2021 – 06.07.2021 over BFNP. The GSD of the orthomosaics used was 0.1m. For the computed temporal changes from DESIS, a suitable spectral index MCARI that matches very well with field-collected measurements was selected. Additionally, from the S2 time series, CVI difference between June 2019 and June 2021 that closely matches with DESIS overpass dates were selected. S2 CVI difference was resampled and rescaled to match with DESIS pixel size for comparison. Further, for these two indices defined thresholds that clearly denotes negative changes in conifers: ($p \leq -0.01$) for DESIS MCARI and ($p \leq -0.35$) for S2 CVI were considered.

The two indices were combined to spatially detect changes within conifers named ‘combined detection index.’ A buffer of one pixel is applied to evaluate if accuracy is improved. Improving the overall accuracy also works with few methods like applying buffer to pixels and other morphological operators [88,89]. An accuracy is generated by examining combined detection index pixels that intersects with ground truth infested samples. Occurrence of event or no events are calculated using predicted indices measurement and reference ground truth datasets to estimate True Positives (TP), False Positives (FP). Accuracies are assessed in two ways (1) with respect to area coverage (2) with respect to number of polygons to see changes detected.

$$\text{Overall accuracy} = \frac{\text{Total number of combined detection index area / polygons}}{\text{Total number of infested area / polygons}} \quad (2)$$

The results acquired are validated and explained in further section 3.

3. RESULTS

3.1 Seasonal changes from S2 CVI time series

Spatio-temporal transition in conifers stands were assessed for S2 MSI from 2017 to 2021 by evaluating results of vegetation vitality index CVI and other individual indices. These indices show varied vegetation patterns observed between healthy vs stressed conifers over time. Each index was mapped with a specific bio-physical property that shows patterns of change in vegetation seasonally. S2 MSI does not have a balanced count in number of datasets due to longer time lag in minimal cloud cover acquisitions for example the datasets in time series had 9 summer days, 6 spring days and 5 fall days from 2017 to 2021. As per year, number of days count were 2 in 2017, 4 in 2018, 6 in 2019, 7 in 2020 and 1 in 2021, with which time series for each index were plotted sorted by JD order as shown in Table 4.

Table 4. JD labeled for S2 MSI time series

S2 MSI Time series	Season	JD
08.04.2020	Spring	099
19.04.2019	Spring	109
24.04.2019	Spring	114a
23.04.2020	Spring	114b
18.05.2020	Spring	139
29.05.2018	Spring	149
03.06.2019	Summer	154
17.06.2021	Summer	168
28.06.2019	Summer	179
03.07.2018	Summer	184
13.07.2017	Summer	194
23.07.2019	Summer	204
06.08.2020	Summer	219
21.08.2020	Summer	234
27.08.2018	Summer	239
16.09.2018	Fall	259a
15.09.2020	Fall	259b
21.09.2019	Fall	264a
20.09.2020	Fall	264b
26.09.2017	Fall	269

S2 derived indices shows spatial patterns distributed among conifers in the BFNP. The indices from S2 provides adequate results due to added SWIR range information, unlike DESIS data with no SWIR bands. From the patterns identified, only a few changes can be detected in the conifers due to the different seasons. With this confirmation, it will be feasible to directly attribute major differences in VIs to changes in forest status. Subtle changes over time are plotted against JD of year to monitor variations. S2 results signify not much of seasonal changes are observed among conifers posing a hypothesis that any changes observed in trees could also be due to biotic or abiotic factors. It is evident that most changes occurred in forest during 2019-2020 are due to a major infestation outbreak in 2018 followed by a continuous drought [57]. It was verified with meteorological information that 2019 was the hottest and dry year with 350mm lower precipitation than average [40], thus justifying change in vegetation patterns.

Looking at the differences between the infested and non-infested areas, the VIGreen index reflecting leaf pigment bio-physical characteristics shows visible changes compared to NDVI and NDRE that shows minimal variations in conifers. The patterns of changes for 2017, 2018, and 2019 show smaller changes over years and 2020 has some fluctuations. Results shows that most of the differences are visible in May-June and during the September months [90]. From the spatial patterns of mean CVI as shown in Figure 10 and associated plots between healthy vs stressed conifers indices as shown in Figures 11,12,13 and 14. In (1) 2017, there are smaller difference in July and September (2) 2018 has a smaller difference in May and no difference in July, August, September (3) 2019 shows a slight variation in April, small differences in June, and larger changes in July and September.

Mean CVI showed significant changes between healthy vs. stressed conifers that are closely associated with mean values of VIGreen index. These negative values identify subtle changes in conifers that might have been influenced by the outbreak of bark beetle activity. Single indices shows higher differences in 2020 and 2021 that are more visible than no changes seen in other years but when combining them as CVI most differences are exposed. Vegetation degradation could also be due to several other external environmental factors that affect the trees showing minimal foliage cover and therefore, differences between indices are assessed. These changes are later verified with ground truth reference data using difference maps calculated between two summer months of S2 that closely matches with satellite overpass dates of DESIS.

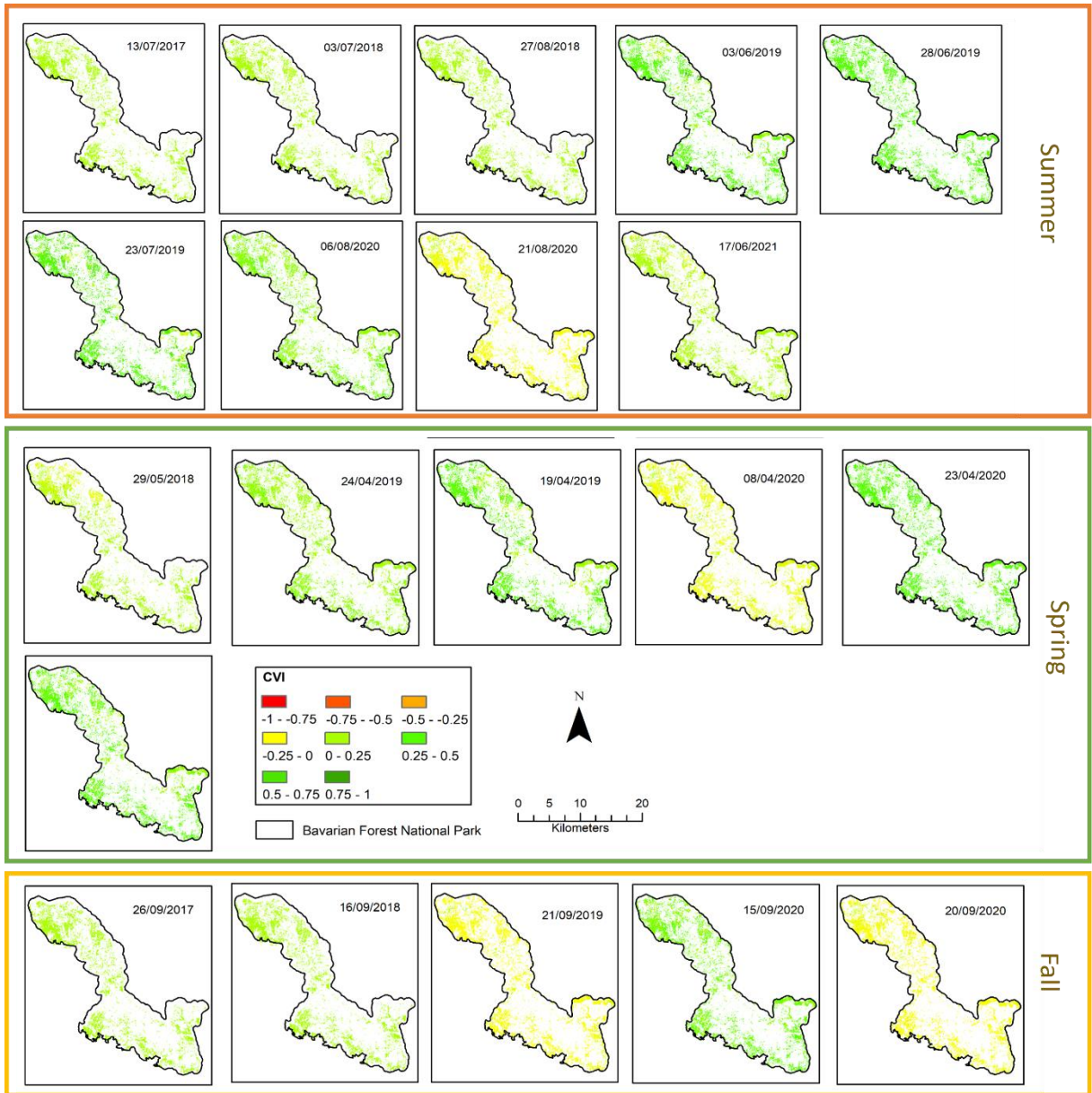


Figure 10. Mean CVI mapped for S2 MSI season wise

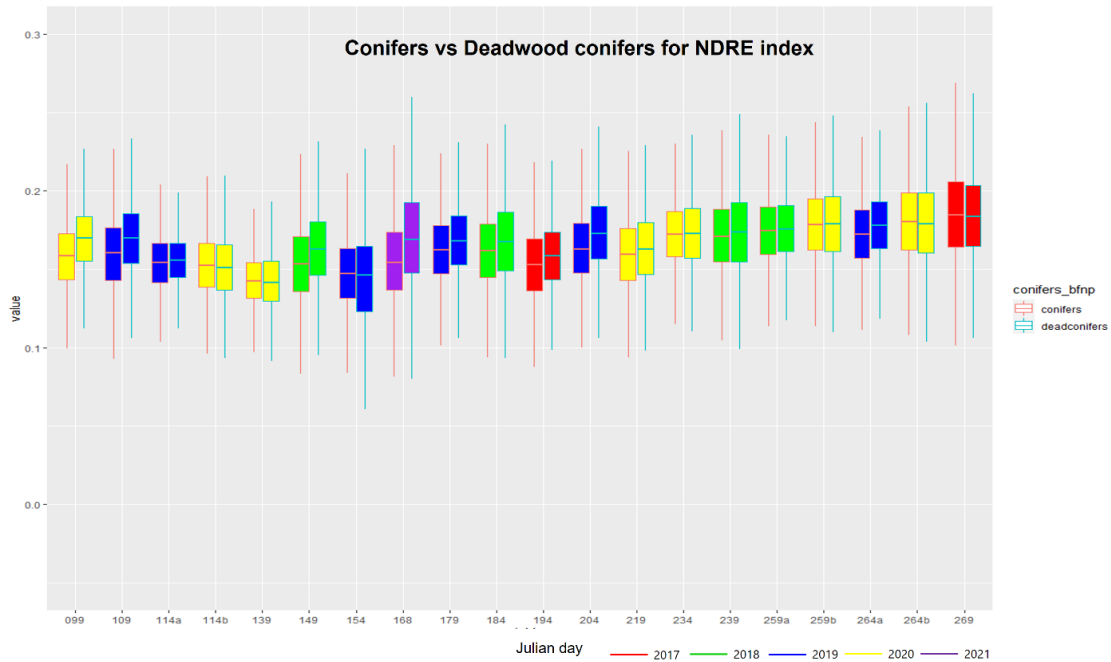


Figure 11. Comparison of S2 NDRE index between Conifers vs stressed conifers.

From NDRE, highest differences in 2021 are observed. Almost no changes visible in JD 234 – 259, and most changes visible JD 99, 109, and 158-219.

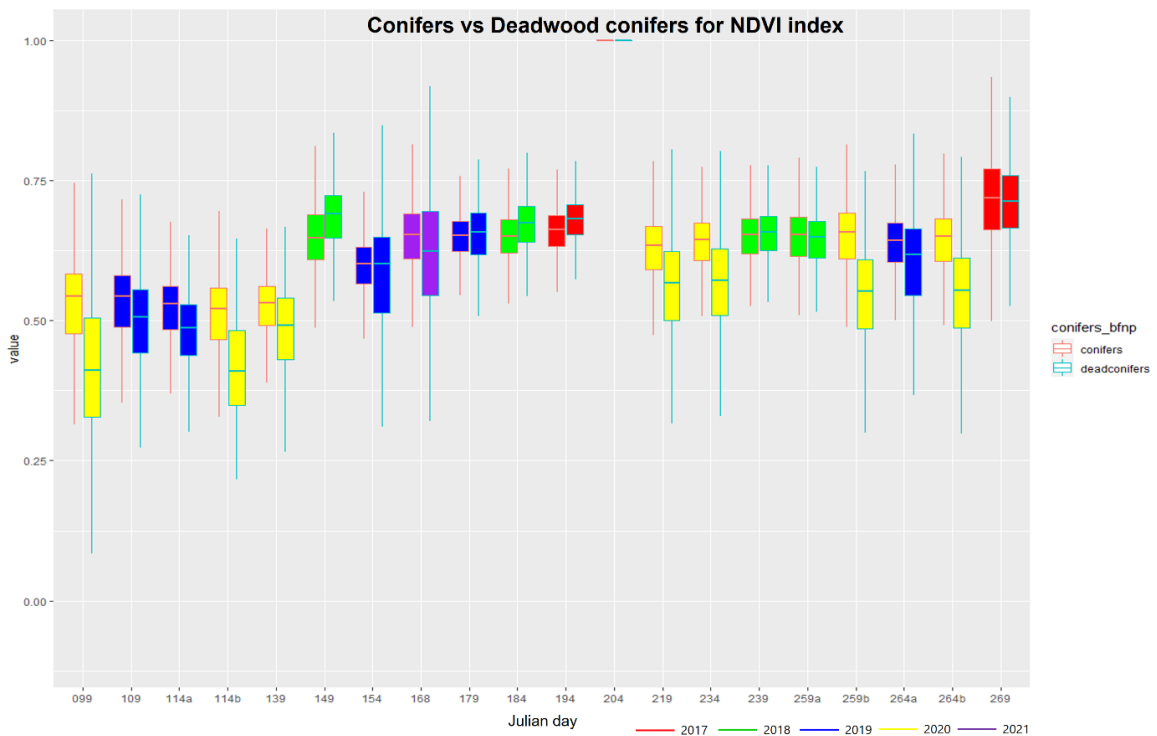


Figure 12. Comparison of S2 NDVI index between Conifers vs stressed conifers.

NDVI shows Highest difference in 2020 and without considering 2020, most changes visible between JD 109-194, and no changes are visible in JD 239 – 269.

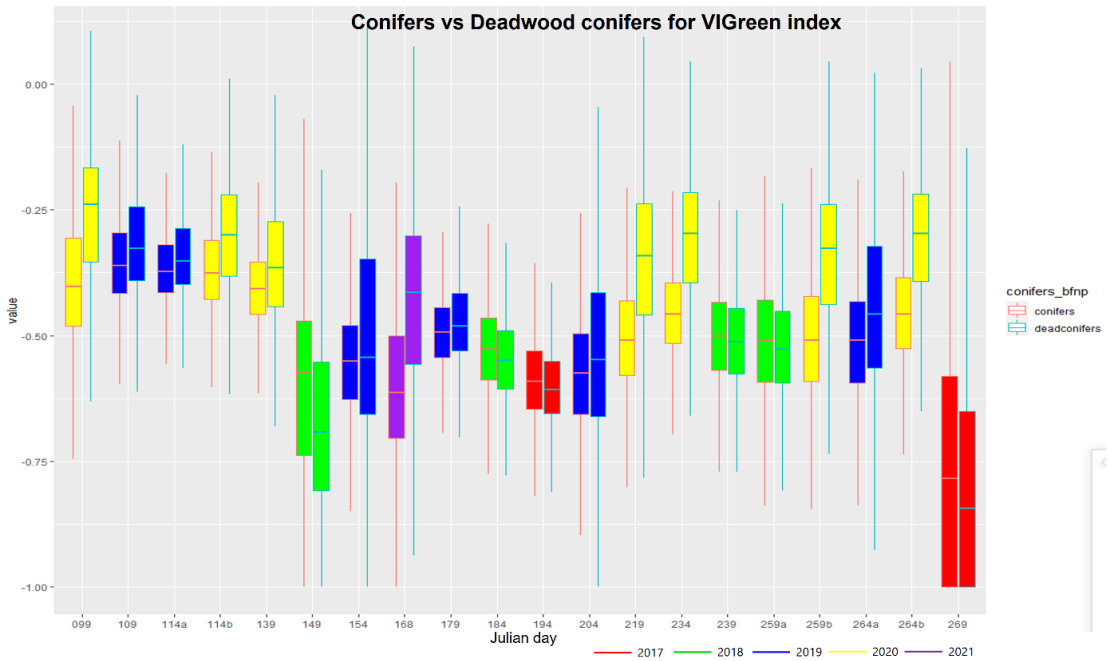


Figure 13. Comparison of S2 VIGreen index between Conifers vs stressed conifers.

Highest difference in 2020 and 2021. Without considering 2020 & 2021, most changes are visible in JD 99-149 and 264 – 269, and almost no changes are visible in JD 154-259.

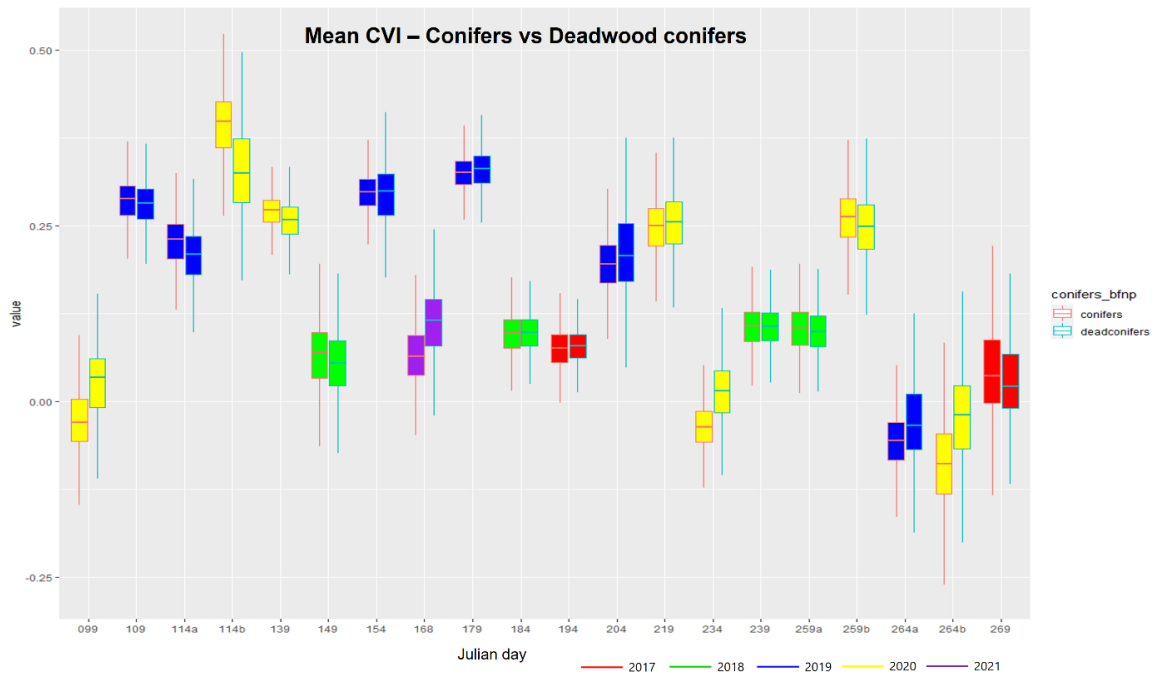


Figure 14. Comparison of S2 mean CVI values between Conifers vs stressed conifers.

Highest difference observed in 2020 and 2021.

3.2 Temporal change estimated from DESIS narrowband VIs

Several narrowband VIs were tested with DESIS to identify suitable indices that fit for this study. Inter-annual change in conifers vegetation was calculated by computing each narrowband index for June 2019 and June 2021 datasets and then deriving a difference image to check its correspondence with the bark beetle infested areas. Scale for all difference maps were normalized and negative values which potentially indicate changes occurred within two years are analyzed. The negative changes represented in red denotes stressed vegetation due to post infestation of bark beetle attack and drought factor from 2018 to 2019. Mainly all the narrowband VIs were examined closely to see if all results were closely relevant with respect to bio-physical property and if they were all capable to highlight changes inside the forest. Additionally, to support the assessment, a few specifications about the behavior of each narrowband VI in correspondence with infested regions is tabulated in Table 5 below.

Table 5. Narrowband indices for temporal change estimation using DESIS

Narrowband VIs	Correspondence of negative change in index with infested areas	Reason
PSRI	Not matching	Increase in PSRI denotes an increase in canopy stress. Physiological stress behavior for conifers varies with crown spatial coverage and chlorophyll content. Sometimes PSRI is more suitable for broadleaf canopies [68].
PRI	Not matching	The index tends to get highly affected by more background features as infested canopy has sparser or no foliage cover. It is also affected by leaf pigment levels and other structural variables [91].
MRESR	Matches partially	It uses red-edge and incorporates a correction for leaf specular reflection.
GI	Not matching	Needles of conifers show minimal change during season affecting chlorophyll absorption in green.
SR	Not matching	This index suits well for vegetation with dense foliage coverage. It is sensitive to background variables like soil, atmospheric effects and viewing angle.

ARI1	Not matching	Anthocyanins are responsible for coloration and indicates plant stress. Reflectance of anthocyanins is observed higher around 550nm and reflects only chlorophyll near 700nm. As conifers needles show minimal foliage cover, this index is not well suited [92].
CRI1	Matches partially	Higher chlorophyll reflectance near 550nm than carotenoids in needles or maybe highly sensitive to growing or young leaves during early summer.
CRI2	Not matching	It is slightly modified than CRI 1, where effect of chlorophyll is reduced by reciprocal of 700 nm denoting the concentration of only carotenoids.
VREI1	Matches partially	With reference to spectral response curve, vegetation stress indication (inflection point observed near red edge region).
REPI	Matches partially	Chlorophyll absorption and leaf internal scattering influences change in index but matches partially due to red edge range [80].
MRENDVI	Matches partially	Includes red edge range but difficult to interpret LAI.
MCARI	Matches well	Index is potential to detect sensitivity of LAI changes[81,93]. It is influenced by chlorophyll and LAI chlorophyll interaction proving a good fit for monitoring temporal changes in vegetation [54].
NDRE	Matches partially	It is a sensitive index to monitor chlorophyll content in leaves but more suitable for broadleaf canopies than conifers which has less volume and stand density. Also, it is observed less sensitive to spatial changes [94].
NDVI	Not matching	The structural nonlinear index is sensitive to background reflectance and difficult to interpret low LAI (leaf area coverage). It is well suited for broad leaf structures.

BFNP has a complex heterogeneous forest cover with a lot of understory influence observed during spring and early summer. In general, most of the retrieved narrowband VIs potentially matches for chlorophyll bio-physical property. This is due to the influence of the red-edge region that eliminates most of the background effects and crown shadows in closed forest canopies, especially in conifers [78]. MCARI, out of all chlorophyll indices, performs well proving as a suitable spectral index for this study. Chlorophyll component in deciduous or mixed forest types are greatly accounted for with larger tree crown density, foliage cover, or volume. But for the conifers, phenological changes reflect from needle chlorophyll content and crown LAI [54]. There may be minimal crown density in needles thus showing sparse matching with structural or leaf pigment properties which is in turn well suited for broadleaf canopies having intense crown volume and foliage. Spatially mapped temporal changes are shown from Figures 15 to 28. As few narrowband VIs shows varied minimum/maximum value range each VIs were normalized separately based on histogram measures. They were categorized as negative change, no change, and change where negative changes indicate the least values representing changes over time. Those values are checked for correspondence with the infested regions collected from 2019 to 2021. Few narrowband indices listed above were estimated using DESIS and are shown as following.

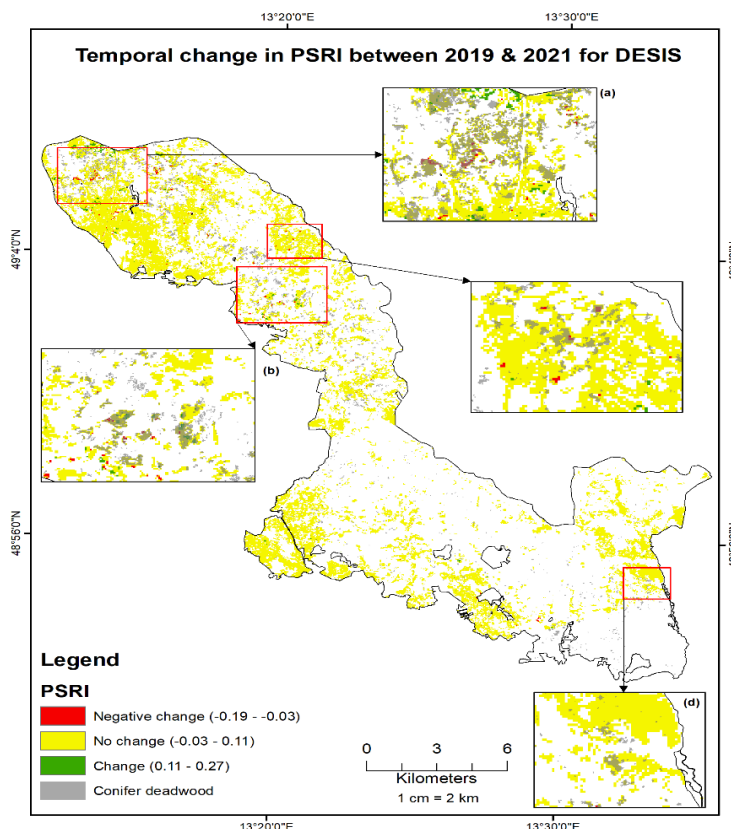


Figure 15. Temporal change calculated for PSRI for DESIS between 2019 and 2021

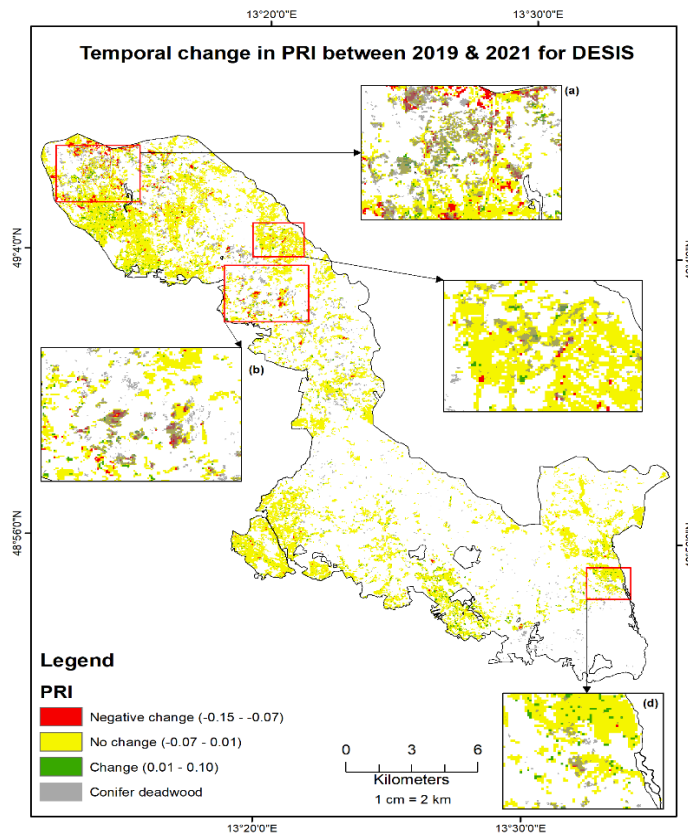


Figure 16. Temporal change calculated for PRI for DESIS between 2019 and 2021

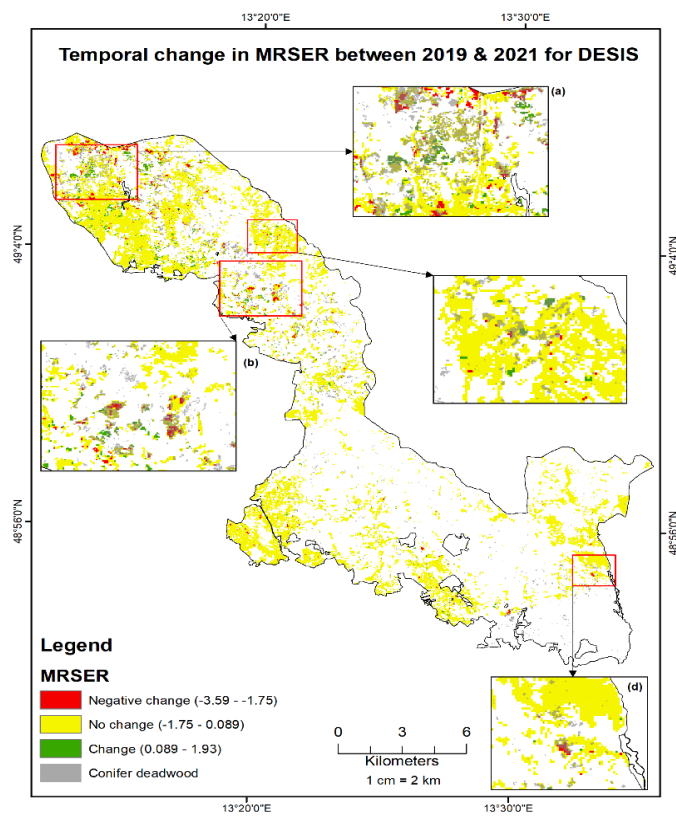


Figure 17. Temporal change calculated for MRSER for DESIS between 2019 and 2021

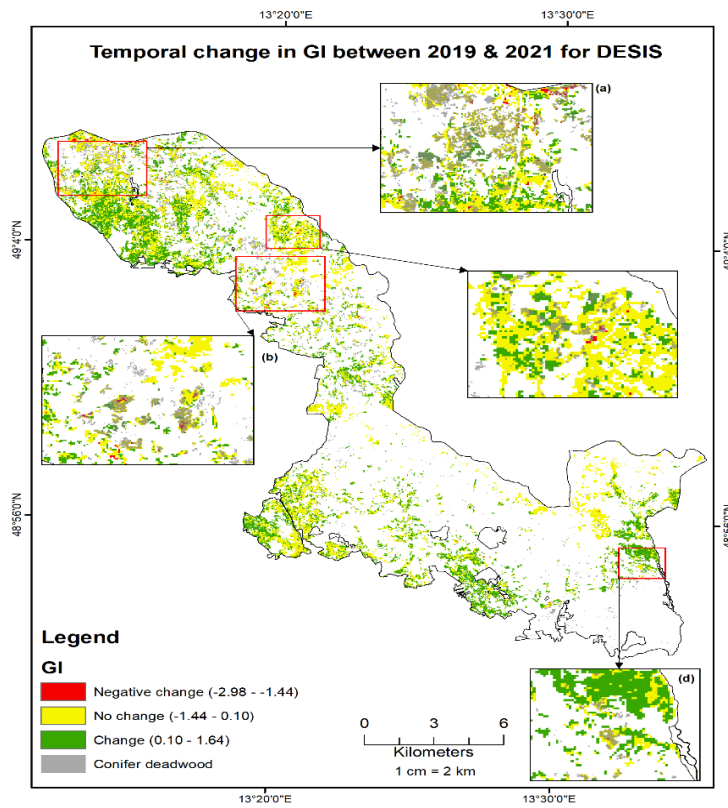


Figure 18. Temporal change calculated for GI for DESIS between 2019 and 2021

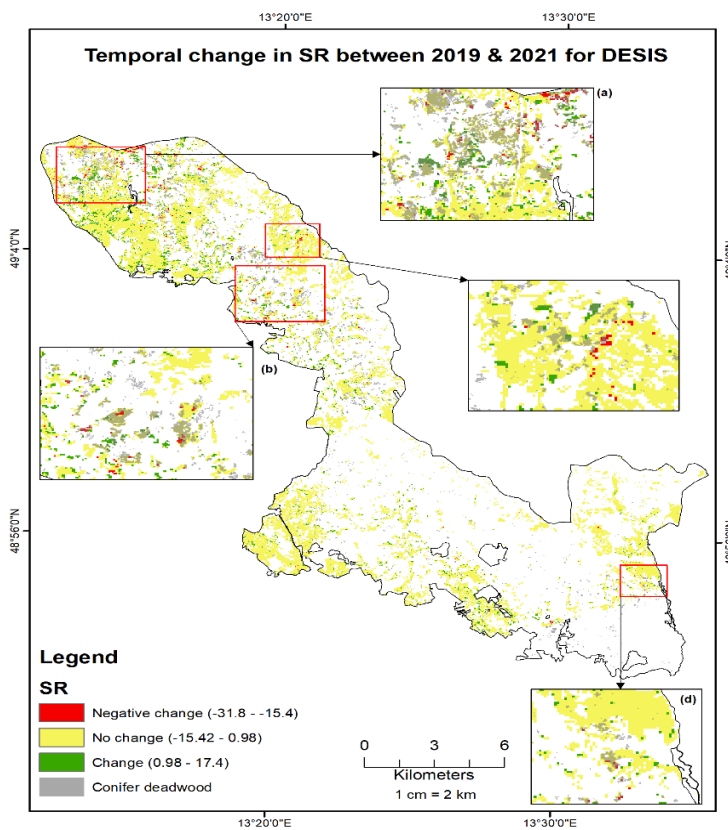


Figure19. Temporal change calculated for SR for DESIS between 2019 and 2021

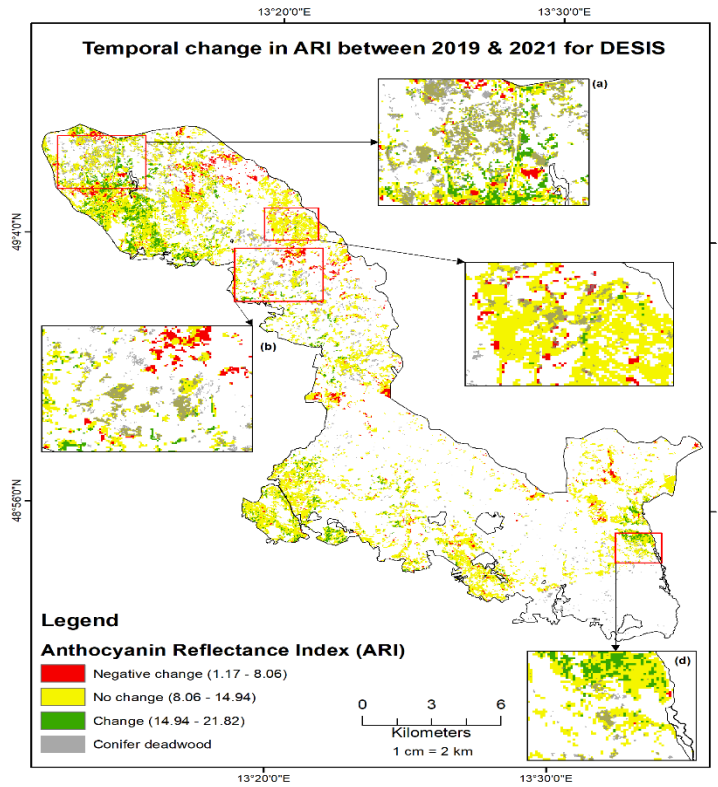


Figure 20. Temporal change calculated for ARI for DESIS between 2019 and 2021

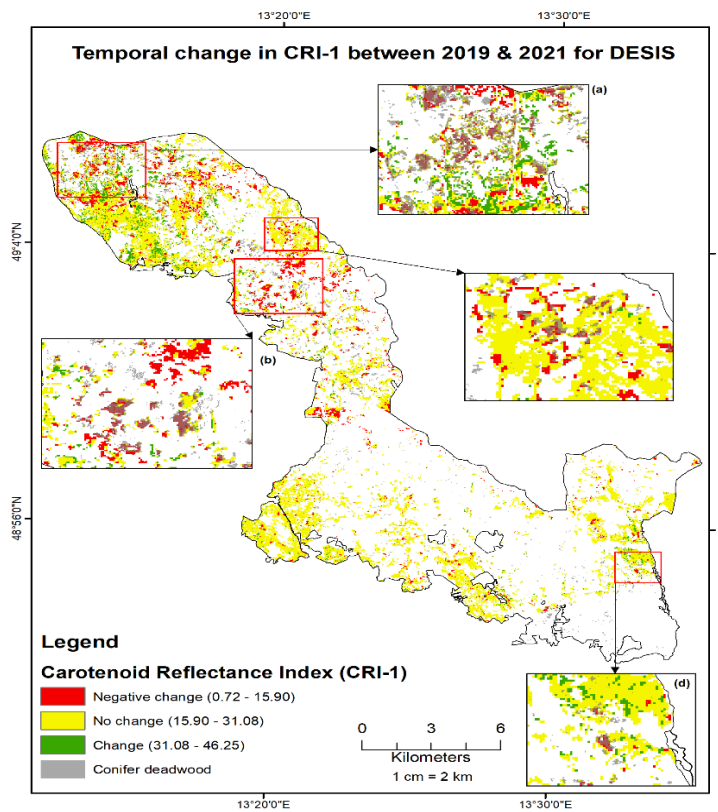


Figure 21. Temporal change calculated for CRI- 1 for DESIS between 2019 and 2021

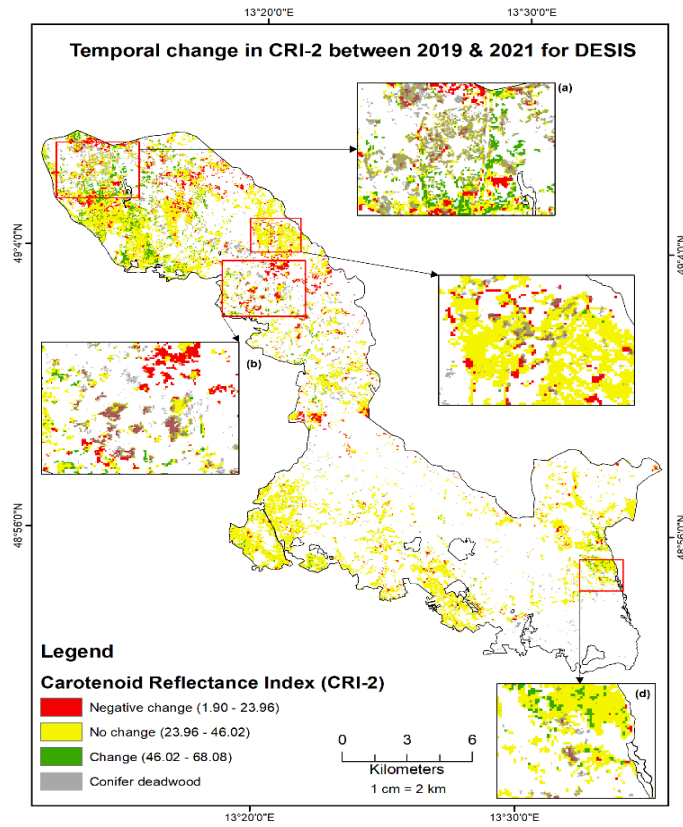


Figure 22. Temporal change calculated for CRI-2 for DESIS between 2019 and 2021

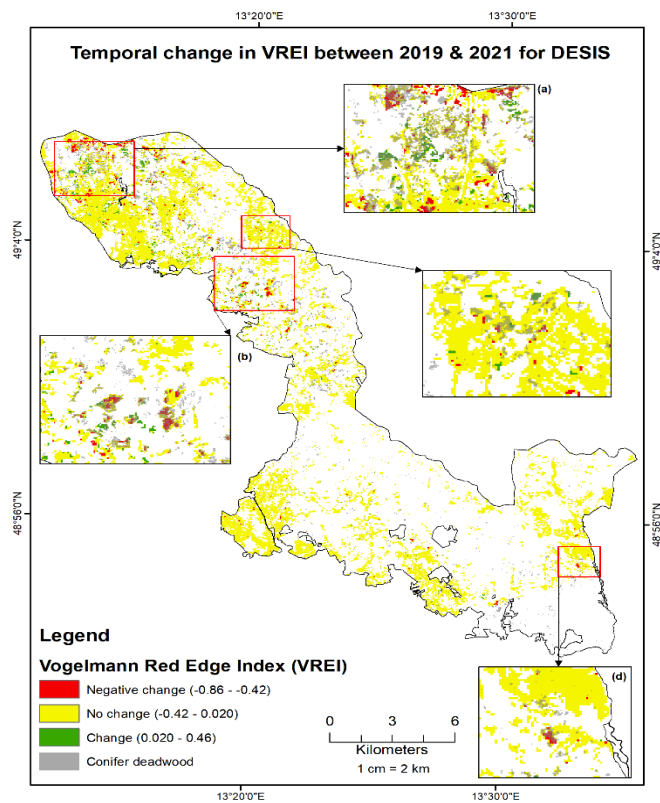


Figure 23. Temporal change calculated for VREI for DESIS between 2019 and 2021

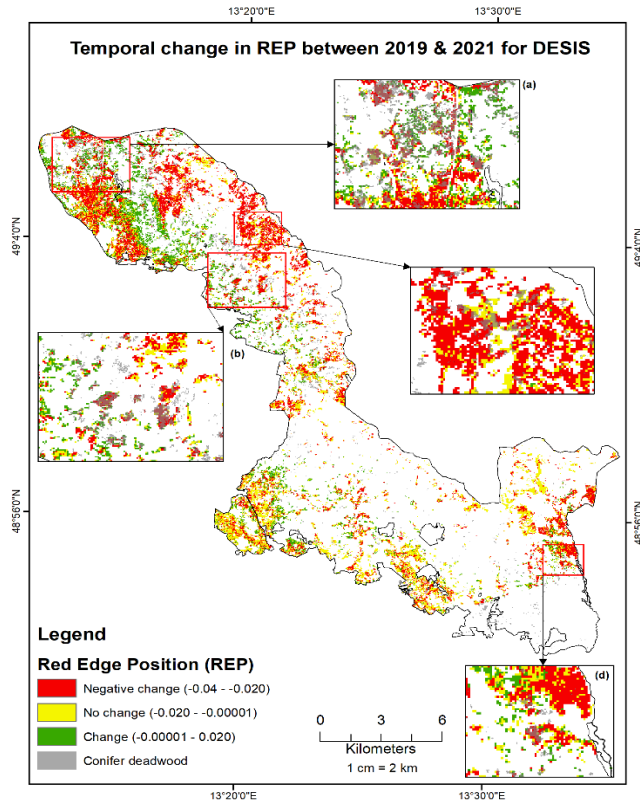


Figure 24. Temporal change calculated for REP for DESIS between 2019 and 2021

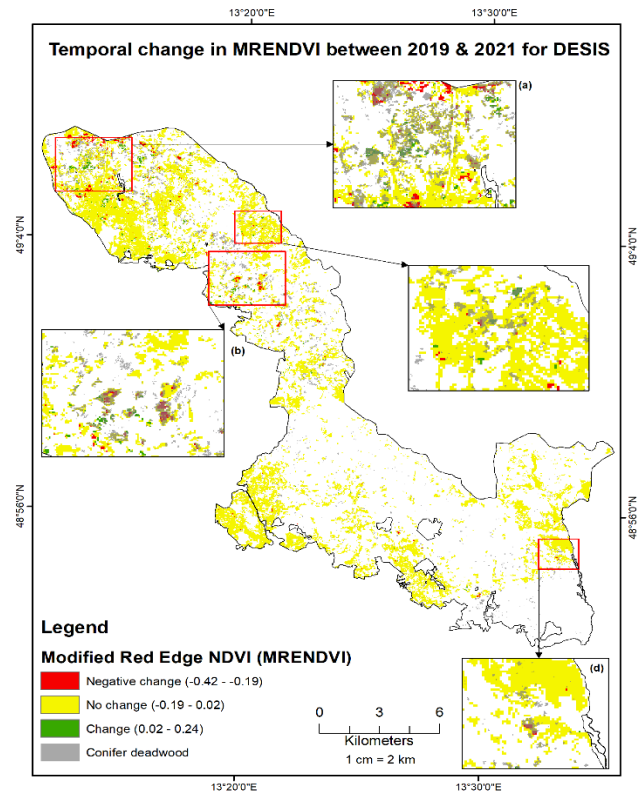


Figure 25. Temporal change calculated for MRENDVI for DESIS between 2019 and 2021

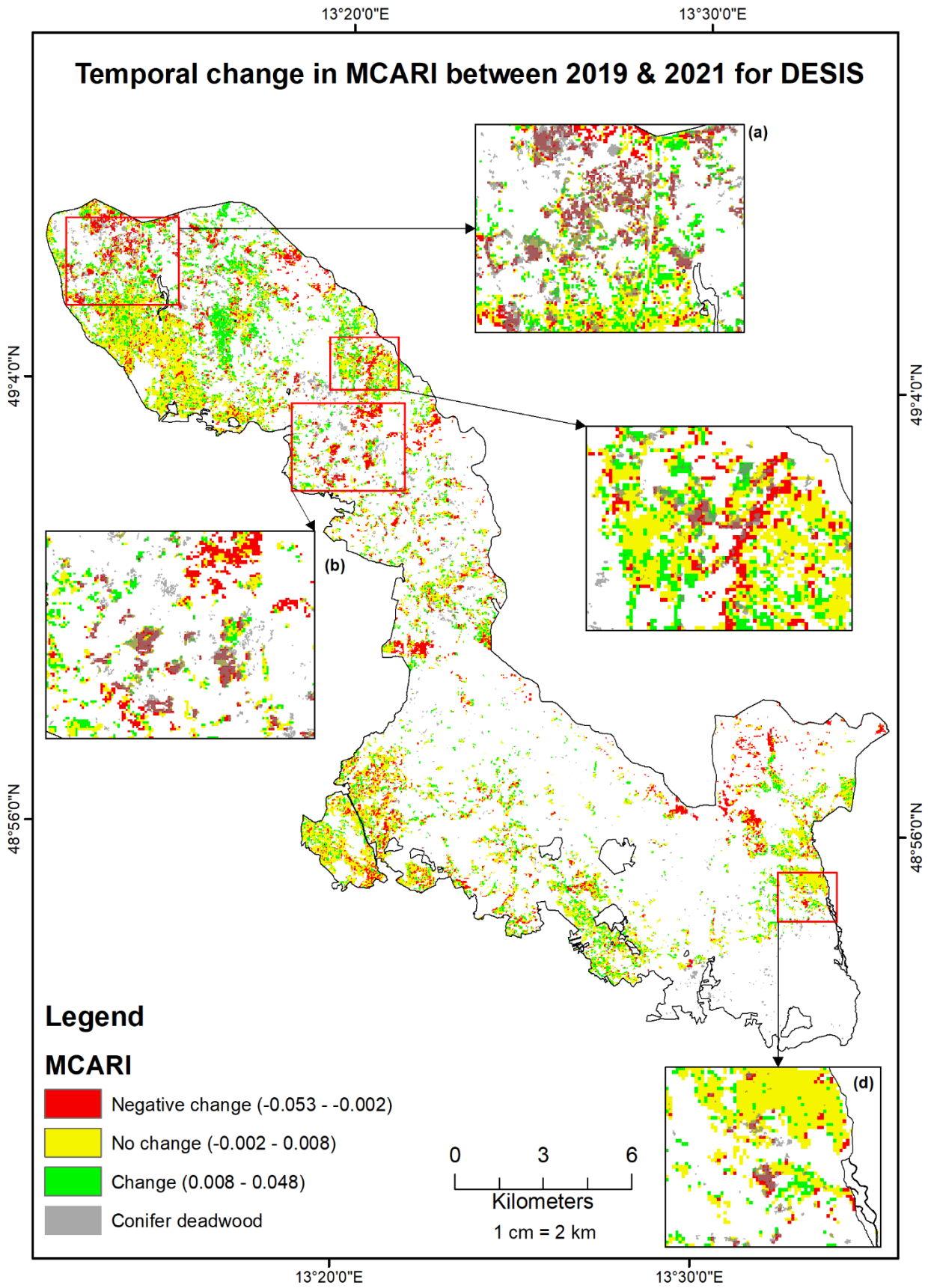


Figure 26. Temporal change calculated for MCARI for DESIS between 2019 and 2021

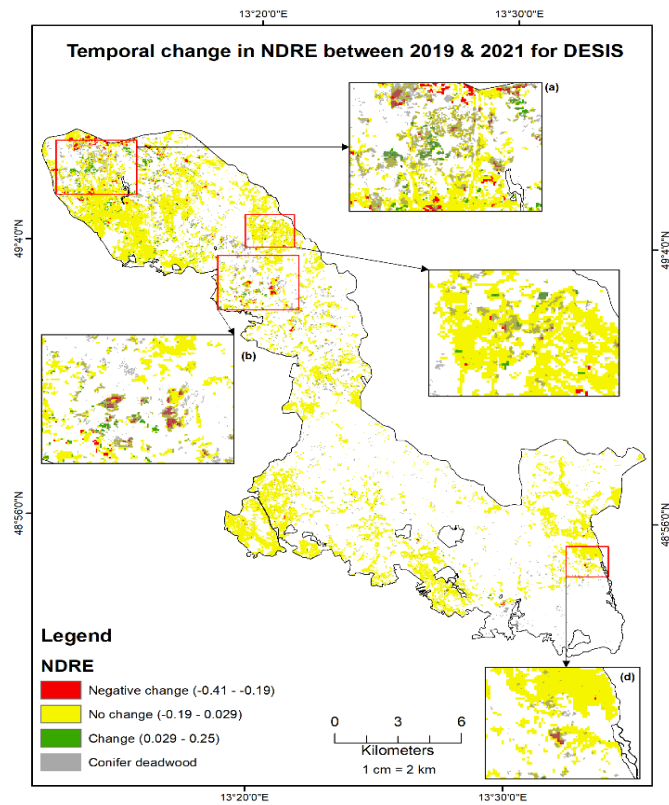


Figure 27. Temporal change calculated for NDRE for DESIS between 2019 and 2021

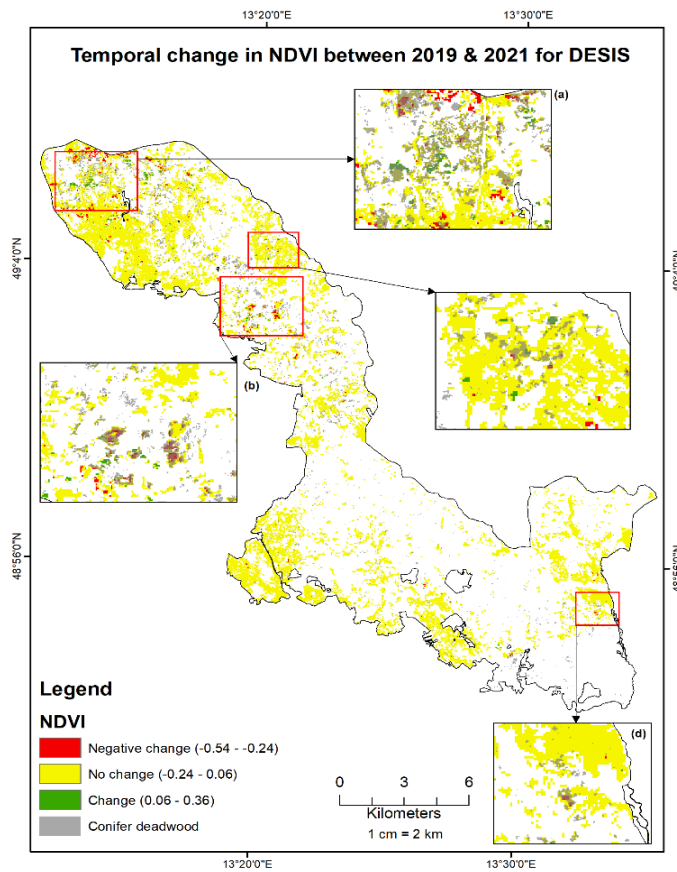
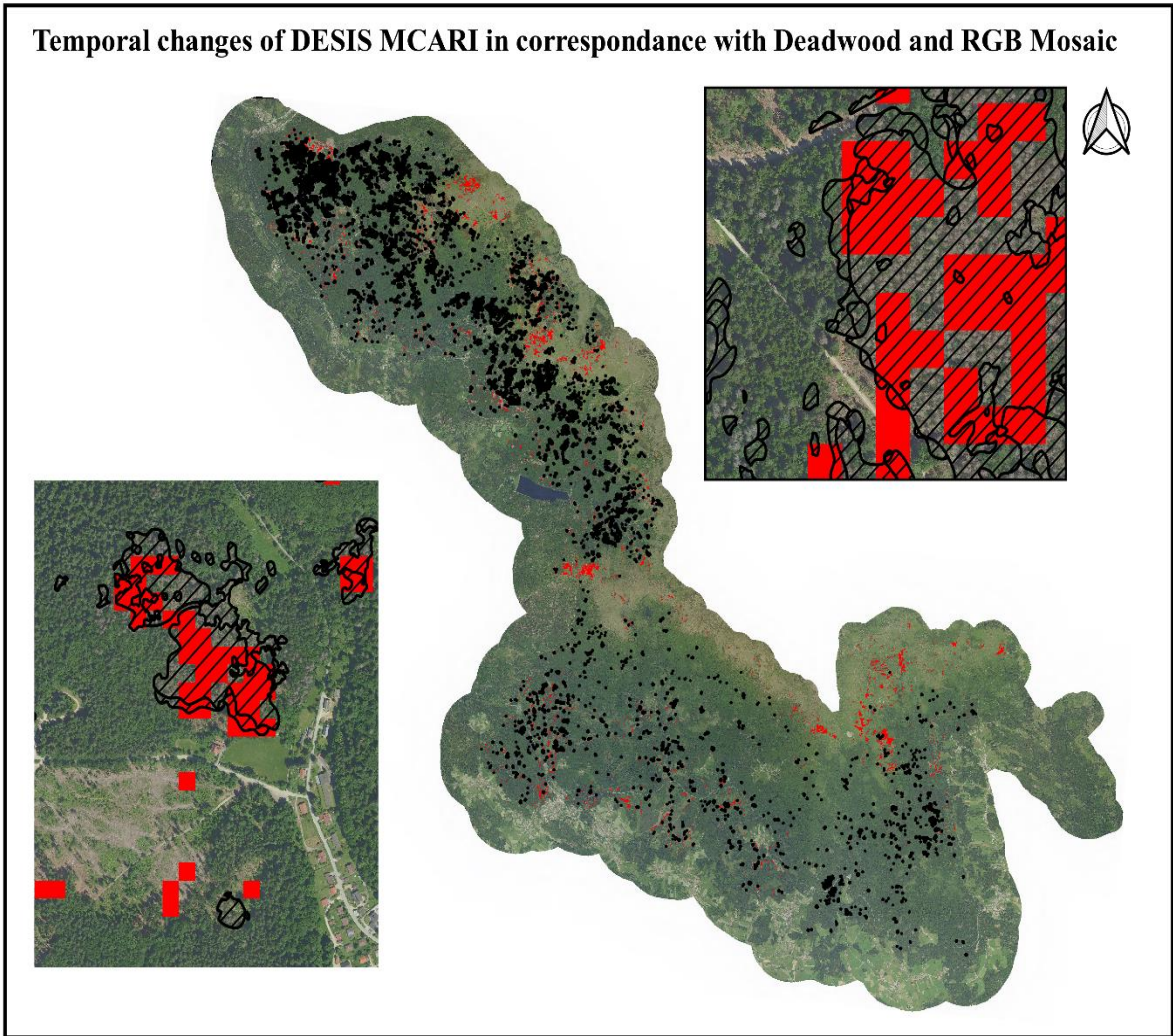


Figure 28. Temporal change calculated for NDVI for DESIS between 2019 and 2021

Assessing each VIs individually, indices with chlorophyll bio-physical properties show spatial similarities when having a closer look at negative changes especially in the northern part of BFNP. The 30m pixels of DESIS distinguishes apparent changes that show a uniform pattern for most of the chlorophyll indices. Few negative changes between these chlorophyll indices are comparable in certain regions where conifers are highly affected inside BFNP. Some interpretations within no change areas maybe the dead spruce trees that are left standing or fallen trees. Later, to avoid errors, ground truth information are matched with a perfectly matching MCARI index after refining its threshold to validate the result. It is evident from the results of narrowband VIs represented in above Figures 15 to 28 that showed significant changes visible in conifers between 2019 to 2021. This could steadily be relevant to relatively higher rates of bark beetle proliferation since 2018 leading to deterioration of conifers health. Statistically, it was also observed that conifers forests mainly spruce stands contribute to major forest loss among all European federal states between 2018 to 2020. Consequently, most of the forest loss were due to drought and beetle infestation [28].

3.3 Threshold definition

For the computed temporal changes from DESIS, a suitable spectral index MCARI that matches very well with field-collected measurements was selected. Additionally, from the S2 time series, CVI difference between June 2019 and June 2021 that closely matches with DESIS overpass dates were selected. S2 CVI difference was resampled and rescaled to match with DESIS pixel size for comparison. After calculating the difference image between DESIS MCARI and S2 CVI, various thresholds were tested for selecting pixels that closely matches with infested regions based on histogram measures. Initially, MCARI with a negative change threshold ($p \leq -0.005$) and CVI with range ($p \leq -0.35$) showed good agreement with the ground truth pixels. The individual matching of pixels with MCARI and CVI indices are represented in Figures 29 and 30 respectively.



Deadwood Areas 2020 & 2021

DESIS MCARI Index for 17.6.2021

MCARI Values ≤ -0.0050

RGB Mosaic Acquisitions from 14.6.2021 to 6.7.2021

Band 1

Band 2

Band 3

0 2.5 5 km



Figure 29. MCARI negative changes matching with orthomosaics and ground truth reference data with ≤ -0.005 threshold.

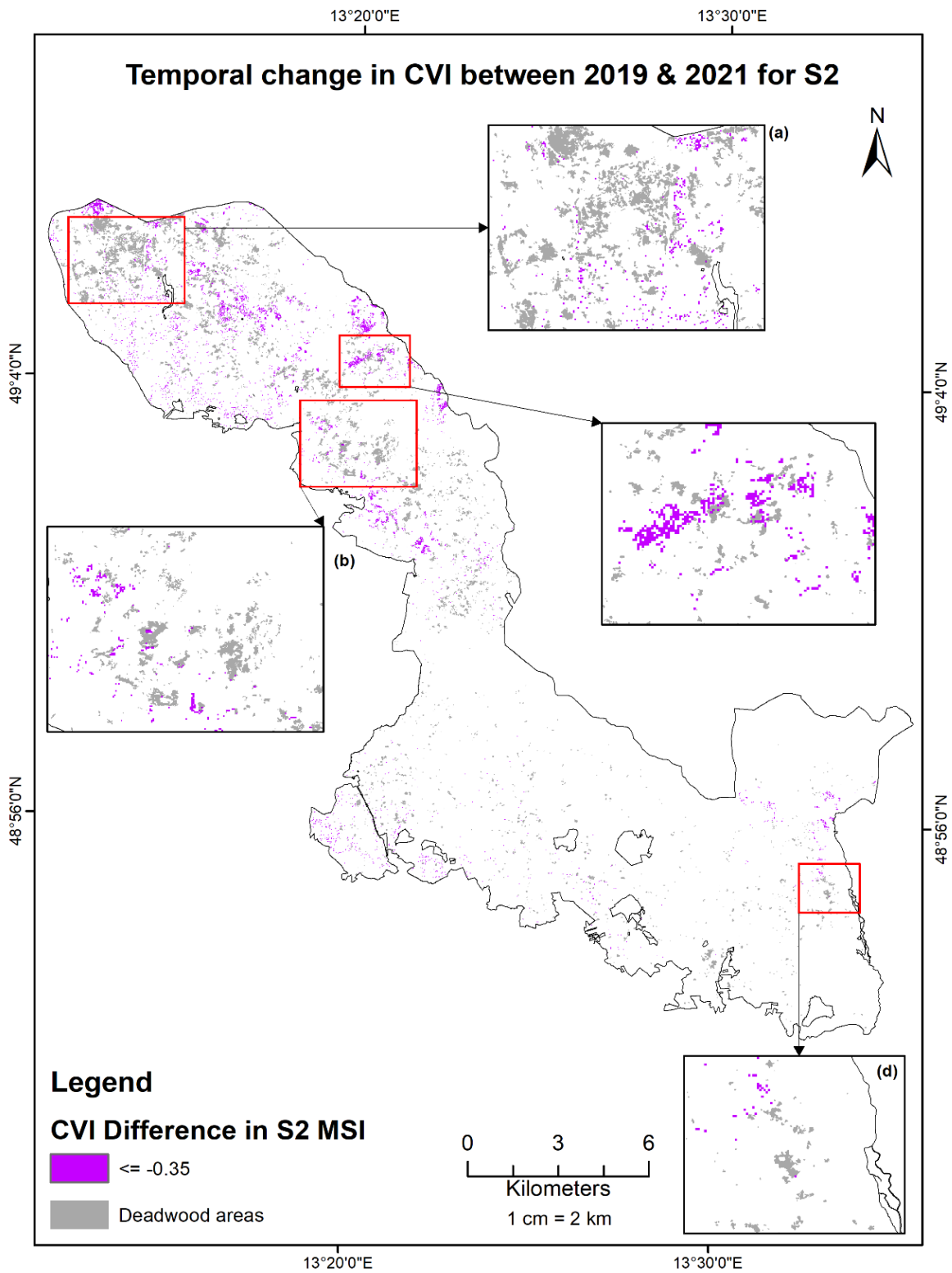


Figure 30. CVI negative changes matching with ground truth polygons with ≤ -0.35 threshold.

Several other threshold levels were also examined out of which MCARI with range ($p \leq -0.01$) and CVI with same range ($p \leq -0.35$) were finalized. The difference of CVI index was resampled to 30 meters to see if there are larger changes when matching with ground truth datasets when compared to DESIS. The combined results provide good coverage from which infested areas that fall within the combination of two indices are identified based on area coverage and polygon count. This method is implemented by adding a buffer of one pixel (i.e., 30 meters) to the combined index, which shows improvement in overall accuracy.

3.4 Validation results

The following sub-sections describe DESIS and S2 product intercomparison results also explains how single products are combined and validated with ground truth reference datasets. Further accuracies calculations based on areal coverage and polygon count are included.

3.4.1 Product intercomparison

The results that include a suitable spectral narrowband index of DESIS and mean CVI from S2 were validated using ground truth information. These datasets include reference polygons as region of interests and high-resolution orthomosaics that clearly shows stressed and cut-down forest stands. In validation, a few sets of procedures were incorporated. Initially, TP and FP were identified by examining the overall accuracies adding two raster indices called “combined detection index.” To obtain this raster, difference is calculated between the summer months of MCARI and CVI matching approximately similar satellite overpass dates. Using this, product intercomparison is performed and results shows if the combination of both datasets are useful to detect changes in conifers. From the combined detection index, pixels that are predicted as infested area and are truly infested represents TP and pixels that are predicted as infested area but not infested represents FP were analyzed. Consequently, the combined index derived by testing different threshold values produced good results with no FP detected.

3.4.2 Analysis of combined detection Index

After matching the pixel size for both indices, overall accuracies were computed using ENVI. The change detection index clearly represents total number of change pixels only after the difference rasters were brought to a similar array dimension of 900*874 with 30 m resolution. The statistics of the combined detection index with applied buffering is analyzed to find out

how many pixels were associated within each category. The statistics retrieved from the raster index were mapped to see distribution of pixels in correspondence with the infested ground truth samples. Using these difference image of 2 indices (MCARI and CVI), a resulting output, as shown in Table 6 was derived at first.

Table 6. Logic for the Combined detection index “MCARI – CVI”

MCARI buffered pixels	CVI buffered pixels	Result
1	1	0 (Agreement)
1	0	1 (detected only by DESIS – uncertain if correct or not)
0	1	-1 (detected only by S2 - uncertain if correct or not)
0	0	0 (Agreement)

As the resulting values 0 might represent either change detected by both or no change detected by both indices, a new raster ($2*MCARI + CVI$) was formed to detect changes as shown in Table 7. In this way, now there are 4 unique cases where each result represents changes of each index.

Table 7. Logic for modified Combined detection index “ $2*MCARI + CVI$ ”

MCARI	CVI	Result
2	1	3 (change detected by both)
2	0	2 (change detected only by DESIS)
0	1	1 (change detected only by S2)
0	0	0 (no change by both)

Analyzing the full conifers area, the results shows that a total of 3432 pixels represents change detected by both sensors, 2932 are change only by DESIS, and 2861 are change by S2 only. No change by both had 777375 pixels, including the background values when evaluated in ENVI. The results of detection index are shown in Figure 31 below. Each change pixels represented good agreement with the ground truth information producing highly reliable results with no false positives based on the defined threshold. A closer look of the combined detection results are shown in Figure 32 displayed over BFNP orthomosaic. All

these results are recorded as binary files while processing where 1 is change detected when combining results and 0 is no change detected. Hence the combined buffer S2 CVI and MCARI file is a binary file with total number of 1's as 9225 (3432+2932+2861) and 0's as 777375 pixels. Supplementary figures representing pixel count acquired from ENVI are shown in Appendix 1.

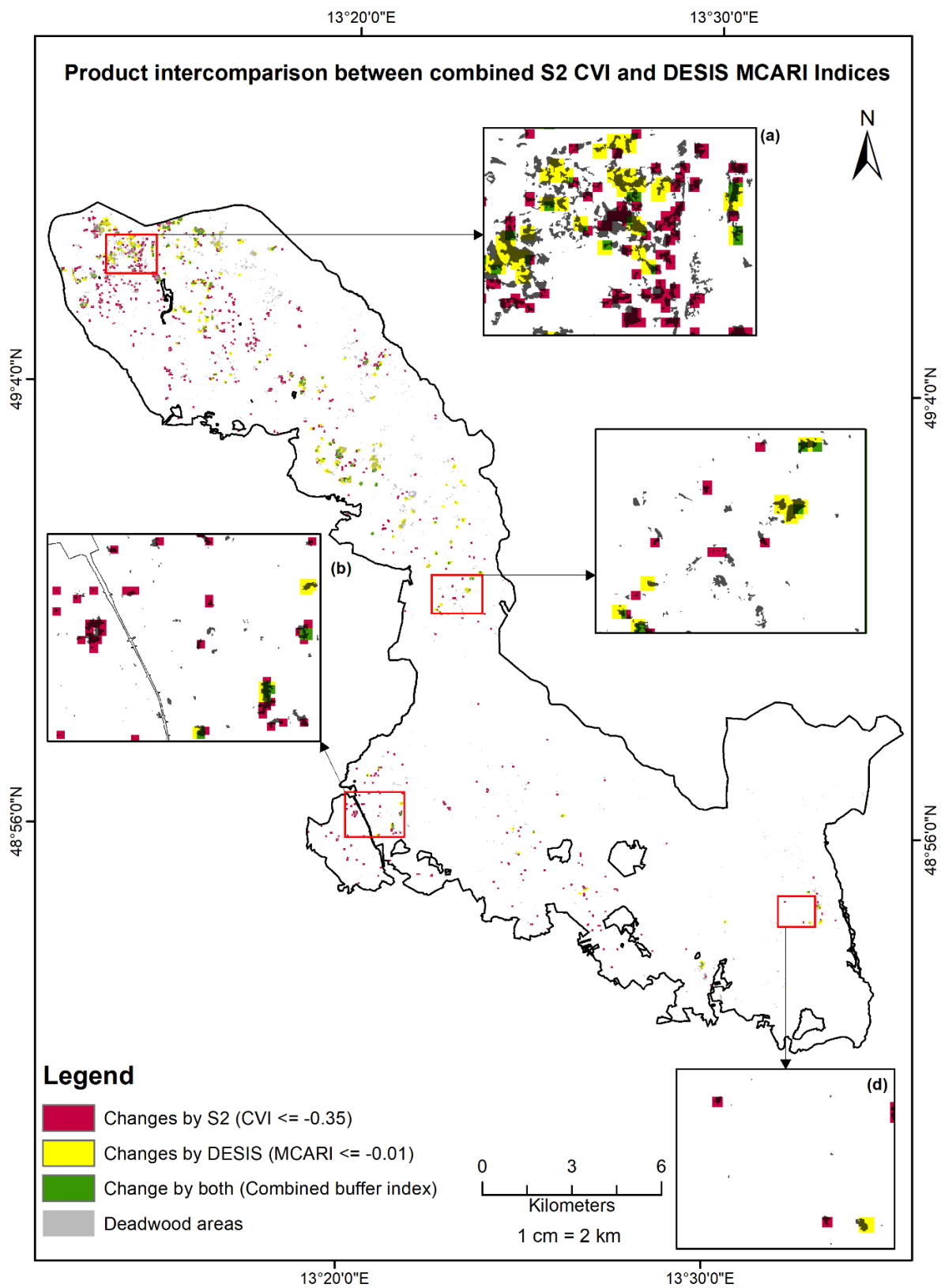


Figure 31. Changes detected using Combined detection index from both DESIS and S2 indices with modified thresholds

CVI and when applying a morphological operator clump class to MCARI and CVI to check if there are improvement in results. All these methods were opted for evaluating raster results and ground truth ROI's converted to a class image. The correct change and no change percentage were examined, and the results were validated based on them. The results are tabulated as shown in Table 8. Outputs from the confusion matrix are added as supplementary figures in Appendix 2.

Table 8. Overall accuracies of percent change and no change compared between original, buffer and clump classes for MCARI and CVI

Index	Correct no change		Correct change	
	MCARI	CVI	MCARI	CVI
Original index	84%	84%	18%	20%
Buffer pixels 30 m	65%	52%	79%	61%
Clump class	68%	71%	70%	86%

The detection rate for the “Correct change” class increased from 18% in MCARI to over 70% when applying a buffer of 1 pixel, or when using the morphological clump operator. This indicates that the spatial co-registration between the ground-truth and the imagery might have a small shift within the mountainous terrain. The overall accuracy decreases as for the buffer and clump cases, the background class is less accurate, and as this is the largest class, this influences the overall accuracy. Hence the values for the large "No Change" class dominate the result for the overall accuracy indicated as 777375 pixels and could not be neglected during confusion matrix calculation using ENVI. It is evident from the results that buffer or clump classes are consistent but the values slightly changes due to influence of background pixels. Therefore, alternatively another method was implemented to check the accuracy by matching vector polygons of detection index with ground truth ROI's using intersect operation from QGIS.

3.4.3.2 Accuracies by matching vectors in QGIS

The predicted detection index was converted into a vector file and intersected with the reference filed collected ROI's. This was to check if the combined approach of S2 CVI and DESIS MCARI effectively corresponds with the infested regions. The calculations were computed based on the area covered and number of polygons that were correctly identified. The vectors were checked to analyze if all polygons overlap with infested areas as shown in raster output.

➤ Accuracies with respect to area coverage:

After intersecting the combined detection index with ground truth ROI's, ratio between two areas were computed to check how much areas were successfully mapped inside affected regions. The area of detection index intersect was 1,774,015 Sq. m and the total area of infestation was 3,273,724 Sq. m. The ratio between the two areas provides that accuracy rate of polygons matching well with infested regions, and it was 54%. Additionally, to improve the accuracy and see if sub-pixel level changes are detectable, a few tiny polygons were excluded from the infested region vector file. For this, only polygons that were > 900 Sq. m (i.e., areas larger than DESIS 30m*30m pixels) were considered, and the resulting area coverage was 2,797,054 Sq.m. Computing the ratio between detection index intersect and area of infested regions with pixel size greater than DESIS its accuracy increased to 63%. The results are also listed in Table 9.

Table 9. Accuracies with respect to area coverage

Description	Area in Sq. Km	Accuracy
Total area covered by combined S2 CVI + DESIS MCARI index that are truly infested	1.77	Accuracy by area = 54%
Total area covered by the in-situ collected infested regions	3.27	
Total area covered by combined S2 CVI + DESIS MCARI index that are truly infested	1.77	Improved accuracy for areas larger than DESIS 30*30 m pixels = 63%
Total area covered by excluding tiny regions (> 900 Sq. m)	2.79	

➤ Accuracies with respect to number of polygons:

The accuracies are checked again based on the number of polygons between the two vector files to see if there are any variations or improvements in accuracies. Initially, all the multi-part polygons were split as single-part polygons to keep distinct count on each feature. The combined detection intersect had 1269 single polygons and the total vector file had 3365 single-part polygons within affected areas. Estimating the ratio between the two yielded an accuracy of 38%. Since there were too many tiny polygons included, the same scale analysis used for computing accuracies by area coverage was applied. Ground truth polygons > 900 Sq.m (30m*30m) were in total 707 and the same was applied for intersect which showed 405 polygons. The output accuracy increased to 57% and the results are tabulated in Table 10. The method was also tested with quarter > 225 Sq.m (15m*15m) and an extended pixel > 2025 Sq.m (45m*45m) limits to see if the accuracy truly improves, and the results are shown in Table 11.

Table 10. Accuracies with respect to number of polygons

Description	No. of polygons	Accuracy
Total number of polygons intersecting combined index detection results	1269	Accuracy by area = 38%
Total number of ground truth polygons within infested area	3365	
Total number of polygons intersecting combined index excluding tiny polygons (>900 Sq. m)	405	Improved accuracy for polygons larger than DESIS 30*30 m pixels = 57%
Total number of ground truth polygons within infested area excluding tiny polygons (>900 Sq. m)	707	

Table 11. Accuracies based on polygon count with varied pixel size

	Polygons within infested areas	Intersect polygons	% Correctly identified
All polygons	3365	1269	38
>225 Sq.m	1439	685	48
>900 Sq.m	707	405	57
>2025 Sq.m	350	208	59

As an inference from these methods using vector files for accuracy assessment, using the combined approach of S2 and DESIS, 54% of the infested area was successfully mapped as affected, and 38% of the single infested regions were identified. When focusing only on infested areas larger than the DESIS pixel, 57% of the affected tree regions were successfully identified, also increasing the correctly mapped area to 63%.

4. DISCUSSION

The overall goal of this study was to identify patterns of change in vegetation especially focussing on the behaviour of conifers with respect to external environmental factors. This was achievable with aggregation of resourceful S2 multitemporal and DESIS multi-annual spaceborne datasets. DESIS proved to be a spectrally high-resolution input data for monitoring temporal changes in vegetation over years whereas S2 measurements after excluding data artifacts or clouds provided essential improvements required for comparison. However, seasonal changes could be improved if time series of S2 are expanded with minimal to no cloud cover acquisitions. The study uses concurrent observations from the BFNP for validation. The method developed for this study allows to assess the correct year of vegetation degradation events by analysing temporal variations referring to loss of healthy conifers canopies detected by analysing VI's of DESIS and S2. Further, quantifying areal measurements with recorded ground truth information provided added value thus representing forest loss due to drought impact and infestation. Inter-annual difference maps between two years of DESIS demonstrated large scale vegetation degradation within the forest in an obvious way. Additionally, S2 seasonal observations consequently showed subtle changes within conifers forest over the years. These multi-temporal spatial patterns of changes in conifers were verified with few readily available map sources like global forest watch which shows good agreement having large-scale canopy loss in conifers [26,28]. Records show that most part of European forests are affected by external disturbance factors but could not be mapped promptly. Hence nationwide systems are being implemented across Europe to maintain records of disturbance events accomplished by several field surveys [95].

Ground truth datasets were considered as an important asset for this study, allowing for a verification of results. Differences in indices that were made comparable between two sensor products and matched further with reference data proves the novelty of the study. Results explicitly presented forest changes identifiable from the combination of indices using DESIS and S2 MSI datasets. Infested trees detection by S2 CVI and DESIS MCARI indices performed the best. However, individual results by S2 CVI and DESIS MCARI alone are mostly complementary. Combination of these two indices works very well where minute changes based on threshold defined proved existence of infested trees. Altering threshold limits for single indices were quite challenging due to spatial resolution of DESIS and S2 but it was managed and cross-verified by overlaying pixels upon orthomosaics that clearly displayed infested tree patches. The polygon detection and area coverage identified within infested regions yielded improved accuracies. Most of the larger polygons fall over infested

patches and single polygons represents trees cut down or windthrow areas. Though there was a slight influence of pixel size, sub-pixel level changes were detectable from DESIS.

The objective behind following this method by interpreting simple differences between the VIs of two years is to show how reliable these indices are when applied to hyperspectral and multispectral datasets in detecting changes. Each index applied for both DESIS and S2 irrespective of bio-physical parameters represented negative changes that are further refined for processing. In general, change detection using a hyperspectral dataset is quite complex compared to multispectral datasets. These could be due to changes that might occur because of spectral aspects as there are numerous contiguous bands [96]. But the difference image from combined indices was more consistent with statistics derived and field observations showing actual regions of vegetation loss. Changes in vegetation species within forest affected by infestation, windthrow, or drought indicates certain magnitude and direction of change that are identified from difference images. Moreover, these negative changes detected from VIs indicate potentially underestimated vegetation change which had happened over past two years. The results were acceptable not only through visual analysis but also by assessing accuracies with ground truth information. In a nutshell, change detection by integrating VIs and using combination of hyperspectral and multispectral sensor datasets to analyse vegetation shift patterns yielded potential outcomes spatially and statistically thus fulfilling objectives of this study.

Additionally, a few limitations faced in this study includes threshold definition, where several tests were run to identify an appropriate range defining event occurrence as true. Since the field information had numerous tiny single polygons, matching pixels of 30 meters to some extent was highly challenging. Interpretation of S2 CVI was derived by observing pattern change from each individual index season wise to see how they behave with respect to its biophysical property. Further, cloud masking showed significant change in spectral response after applying F-mask for S2 time series inclusions from 2017 and 2018, but VIs had influence from cloud shadows.

5. CONCLUSION AND RECOMMENDATION

5.1. Conclusions

In this research work, a novel hyperspectral DESIS dataset in combination with multispectral S2 MSI time series were used to interpret changes in vegetation patterns by determining forest health status within BFNP. From this study, some of the derived conclusions are:

- For DESIS, narrowband indices which focus on chlorophyll bio-physical parameter at red-edge range yielded potential information on negative changes occurring in conifers forests. In particular, MCARI, MRESR, MRENDVI were found useful. Most of the changes are observed near the northern part of the study area having dense young stands of conifers. These negative changes correspond closely to the infested areas that represents changes due to bark beetle attacks. Also, additional similarities between leaf pigment indices (CRI 1 and 2) having were observed. DESIS can therefore detect changes to some extent even with 30-meter GSD and proved that increased pixel size improves overall accuracies. Forest health monitoring from VIs were opted for this study as indices contribute a lot of information by reducing illumination effects or canopy shading aspects. Another goal was to combine the results with multi-temporal S2 acquisitions to produce a combined output to analyse spatial patterns of change in conifers species.
- Further VIs estimated from S2 time series showed seasonal changes within certain areas of the forest. To interpret the correct year of larger infestation, the time series was expanded to check increased stress in conifers vegetation by sorting the datasets as per JD to match with DESIS. Mean of CVI, and other spectral indices were assessed and plotted as mentioned in section 3.1. Sorting JD close to each other enabled to check the differences between every index of S2. The results of 2020 had few fluctuations due to some outliers but 2018 and 2019 looked fine. Higher differences were observed in 2020 and 2021 that were more visible but not much changes were seen in other years. The idea was to see if there were any large changes in years by observing the patterns of CVI. As an average, CVI showed up subtle changes than individual indices but these changes are not much due to seasonal variations. Also, the fact is that external environmental factors, both biotic and abiotic elements could be a driving force for vegetation degradation apart from bark beetle infestation and drought events. For monitoring forest change development over time there are only few datasets available having high temporal resolution like S2 MSI. Though they have comparatively lower number of bands,

some information from SWIR can be obtained which is still seen as a fallback in DESIS.

- Using a combined detection index from DESIS and S2 provided the best information on changes between 2019 and 2021. When validating, the pixel count and area-based approach with ground truth information reflected actual canopy cover loss in conifers that could be due to infestation by bark beetles or other environmental disturbance events. Therefore, a combination of time series data with high spectral resolution data was found to be superior to using only one source of information. DESIS, seen as a high-quality spectrally input dataset when combined with S2 having finer spatial resolution proves to perform well, showing good agreement with ground truth reference observations. It is also inferred from the accuracy results that these two datasets determine their credibility when combined and applied for forest health monitoring studies.

5.2. Recommendations

A few suggestions as future work from this study could be listed as follows:

- Expanding the time series of S2 with more cloud free or improved cloud-masked data for every season may provide consistent seasonal variations with which changes can be detected.
- So far, only indices were used for interpretation of the results which were absolute values retrieved from direct difference between rasters. Another option would be using classification algorithms like Random Forest or using Radiative Transfer models.
- Further inputs from the suitable indices found shall be used for training such models as changes were already identified.

REFERENCES

1. Millar, C.I.; Stephenson, N.L. Temperate Forest Health in an Era of Emerging Megadisturbance. *Science* **2015**, doi:10.1126/science.aaa9933.
2. FAO *Global Forest Resources Assessment 2020: Main Report*; FAO: Rome, Italy, 2020; ISBN 978-92-5-132974-0.
3. Dash, J.P.; Watt, M.S.; Pearse, G.D.; Heaphy, M.; Dungey, H.S. Assessing Very High Resolution UAV Imagery for Monitoring Forest Health during a Simulated Disease Outbreak. *ISPRS Journal of Photogrammetry and Remote Sensing* **2017**, *131*, 1–14, doi:10.1016/j.isprsjprs.2017.07.007.
4. Acharya, R.P.; Maraseni, T.; Cockfield, G. Global Trend of Forest Ecosystem Services Valuation – An Analysis of Publications. *Ecosystem Services* **2019**, *39*, 100979, doi:10.1016/j.ecoser.2019.100979.
5. Ninan, K.N.; Inoue, M. Valuing Forest Ecosystem Services: What We Know and What We Don't. *Ecological Economics* **2013**, *93*, 137–149, doi:10.1016/j.ecolecon.2013.05.005.
6. Krieger, D. Economic Value of Forest Ecosystem Services: A Review. *The Wilderness Society* **2001**, *1615*.
7. Franklin, J.F.; Spies, T.A.; Pelt, R.V.; Carey, A.B.; Thornburgh, D.A.; Berg, D.R.; Lindenmayer, D.B.; Harmon, M.E.; Keeton, W.S.; Shaw, D.C.; et al. Disturbances and Structural Development of Natural Forest Ecosystems with Silvicultural Implications, Using Douglas-Fir Forests as an Example. *Forest Ecology and Management* **2002**, *155*, 399–423, doi:10.1016/S0378-1127(01)00575-8.
8. Schlyter, P.; Stjernquist, I.; Barring, L.; Jönsson, A.; Nilsson, C. Assessment of the Impacts of Climate Change and Weather Extremes on Boreal Forests in Northern Europe, Focusing on Norway Spruce. *Climate Research - CLIMATE RES* **2006**, *31*, 75–84, doi:10.3354/cr031075.
9. Trumbore, S.; Brando, P.; Hartmann, H. Forest Health and Global Change. *Science* **2015**, *349*, 814–818, doi:10.1126/science.aac6759.
10. Gauthier, S.; Bernier, P.; Kuuluvainen, T.; Shvidenko, A.; Schepaschenko, D. Boreal Forest Health and Global Change. *Science (New York, N.Y.)* **2015**, *349*, 819–822, doi:10.1126/science.aaa9092.
11. Weed, A.S.; Ayres, M.P.; Hicke, J.A. Consequences of Climate Change for Biotic Disturbances in North American Forests. *Ecological Monographs* **2013**, *83*, 441–470, doi:10.1890/13-0160.1.
12. FAO and UNEP *The State of the World's Forests 2020: Forests, biodiversity and people*; The State of the World's Forests (SOFO); FAO and UNEP: Rome, Italy, 2020; ISBN 978-92-5-132419-6.
13. Seidl, R.; Schelhaas, M.-J.; Rammer, W.; Verkerk, H. Increasing Forest Disturbances in Europe and Their Impact on Carbon Storage (Vol 4, Pg 806, 2014). *Nature Climate Change* **2014**, *4*, 930–930, doi:10.1038/NCLIMATE2393.
14. Seidl, R.; Thom, D.; Kautz, M.; Martín-Benito, D.; Peltoniemi, M.; Vacchiano, G.; Wild, J.; Ascoli, D.; Petr, M.; Honkaniemi, J.; et al. Forest Disturbances under Climate Change. *Nature Climate Change* **2017**, *7*, 395–402.
15. Senf, C.; Müller, J.; Seidl, R. Post-Disturbance Recovery of Forest Cover and Tree Height Differ with Management in Central Europe. *Landscape Ecology* **2019**, *34*, doi:10.1007/s10980-019-00921-9.
16. ADAPTATION OF FORESTS AND PEOPLE TO CLIMATE CHANGE – A Global Assessment Report — Climate-ADAPT Available online: <https://climate-adapt.eea.europa.eu/metadata/publications/adaptation-of-forests-and-people-to-climate-change-2013-a-global-assessment-report> (accessed on 2 February 2022).
17. Lausch, A.; Erasmí, S.; King, D.J.; Magdon, P.; Heurich, M. Understanding Forest Health with Remote Sensing -Part I—A Review of Spectral Traits, Processes and Remote-Sensing Characteristics. *Remote Sensing* **2016**, *8*, 1029, doi:10.3390/rs8121029.

18. Lausch, A.; Borg, E.; Bumberger, J.; Dietrich, P.; Heurich, M.; Huth, A.; Jung, A.; Klenke, R.; Knapp, S.; Mollenhauer, H.; et al. Understanding Forest Health with Remote Sensing, Part III: Requirements for a Scalable Multi-Source Forest Health Monitoring Network Based on Data Science Approaches. *Remote Sensing* **2018**, *10*, 1120, doi:10.3390/rs10071120.
19. Lausch, A.; Heurich, M.; Fahse, L. Spatio-Temporal Infestation Patterns of Ips Typographus (L.) in the Bavarian Forest National Park, Germany. *Ecological Indicators* **2013**, *31*, 73–81, doi:10.1016/j.ecolind.2012.07.026.
20. Lausch, A.; Fahse, L.; Heurich, M. Factors Affecting the Spatio-Temporal Dispersion of Ips Typographus (L.) in Bavarian Forest National Park: A Long-Term Quantitative Landscape-Level Analysis. *Forest Ecology and Management* **2011**, *261*, 233–245, doi:10.1016/j.foreco.2010.10.012.
21. Potter, K.M.; Conkling, B.L. Forest Health Monitoring: National Status, Trends, and Analysis 2020. *General Technical Report SRS-261* **2021**, *261*, 1–211, doi:10.2737/SRS-GTR-261.
22. Bässler, C.; Förster, B.; Moning, C.; Müller, J. The BIOKLIM Project: Biodiversity Research between Climate Change and Wilding in a Temperate Montane Forest—The Conceptual Framework. *For. Landsc. Res.* **2009**, *7*.
23. Heurich, M. Progress of Forest Regeneration after a Large-Scale Ips Typographus Outbreak in the Subalpine Picea Abies Forests of the Bavarian Forest National Park. *Silva Gabreta* **2009**, *15*, 49–66.
24. Fernandez-Carrillo, A.; Patočka, Z.; Dobrovolný, L.; Franco-Nieto, A.; Revilla-Romero, B. Monitoring Bark Beetle Forest Damage in Central Europe. A Remote Sensing Approach Validated with Field Data. *Remote Sensing* **2020**, *12*, 3634, doi:10.3390/rs12213634.
25. Coops, N.; Johnson, M.; Wulder, M.; White, J. Assessment of QuickBird High Spatial Resolution Imagery to Detect Red Attack Damage Due to Mountain Pine Beetle Infestation. *Remote Sensing of Environment* **2006**, *103*, 67–80, doi:10.1016/j.rse.2006.03.012.
26. Vizzuality Forest Monitoring, Land Use & Deforestation Trends | Global Forest Watch Available online: <https://www.globalforestwatch.org/> (accessed on 2 February 2022).
27. Buras, A.; Rammig, A.; Zang, C.S. The European Forest Condition Monitor: Using Remotely Sensed Forest Greenness to Identify Hot Spots of Forest Decline. *Frontiers in Plant Science* **2021**, *12*.
28. Thonfeld, F.; Gessner, U.; Holzwarth, S.; Kriese, J.; da Ponte, E.; Huth, J.; Kuenzer, C. A First Assessment of Canopy Cover Loss in Germany's Forests after the 2018–2020 Drought Years. *Remote Sensing* **2022**, *14*, 562, doi:10.3390/rs14030562.
29. Holzwarth, S.; Thonfeld, F.; Abdullahi, S.; Asam, S.; Da Ponte Canova, E.; Gessner, U.; Huth, J.; Kraus, T.; Leutner, B.; Kuenzer, C. Earth Observation Based Monitoring of Forests in Germany: A Review. *Remote Sensing* **2020**, *12*, 3570, doi:10.3390/rs12213570.
30. Shi, Y.; Skidmore, A.; Holzwarth, S.; Heiden, U.; Heurich, M. Mapping Individual Silver Fir Trees Using Hyperspectral and LiDAR Data in a Central European Mixed Forest. *International Journal of Applied Earth Observation and Geoinformation* **2021**, *98*, 102311, doi:10.1016/j.jag.2021.102311.
31. Bässler, C.; Müller, J.; Dziöck, F. Detection of Climate-Sensitive Zones and Identification of Climate Change Indicators: A Case Study from the Bavarian Forest National Park. *Folia Geobotanica* **2010**, *45*, 163–182, doi:10.1007/s12224-010-9059-4.
32. *Hyperspectral Remote Sensing of Vegetation*; Thenkabail, P.S., Lyon, J.G., Eds.; CRC Press: Boca Raton, 2011; ISBN 978-0-429-19218-0.
33. Hill, J.; Buddenbaum, H.; Townsend, P. Imaging Spectroscopy of Forest Ecosystems: Perspectives for the Use of Space-Borne Hyperspectral Earth Observation Systems. In; 2019; pp. 257–292 ISBN 978-3-030-24909-0.
34. Kayet, N.; Pathak, K.; Chakrabarty, A.; Singh, C.P.; Chowdary, V.; Kumar, S.; Sahoo, S. Forest Health Assessment for Geo-Environmental Planning and Management in Hilltop Mining Areas

- Using Hyperion and Landsat Data. *Ecological Indicators* **2019**, *106*, doi:10.1016/j.ecolind.2019.105471.
35. Kovacs, J.; Wang, J.; Flores-Verdugo, F. Mapping Mangrove Leaf Area Index at the Species Level Using IKONOS and LAI-2000 Sensors for the Agua Brava Lagoon, Mexican Pacific. *Estuarine Coastal and Shelf Science* **2005**, *62*, 377–384, doi:10.1016/j.ecss.2004.09.027.
 36. Marshall, M.; Thenkabail, P.; Biggs, T.; Post, K. Hyperspectral Narrowband and Multispectral Broadband Indices for Remote Sensing of Crop Evapotranspiration and Its Components (Transpiration and Soil Evaporation). *Agricultural and Forest Meteorology* **2016**, *218–219*, doi:10.1016/j.agrformet.2015.12.025.
 37. Krutz, D.; Sebastian, I.; Eckardt, A.; Venus, H.; Walter, I.; Günther, B.; Säuberlich, T.; Neidhardt, M.; Zender, B.; Lieder, M.; et al. DESIS - DLR Earth Sensing Imaging Spectrometer for the International Space Station ISS. In Proceedings of the Sensors, Systems, and Next-Generation Satellites XXII; SPIE, September 25 2018; Vol. 10785, pp. 79–87.
 38. Alonso, K.; Bachmann, M.; Burch, K.; Carmona, E.; Cerra, D.; de los Reyes, R.; Dietrich, D.; Heiden, U.; Hölderlin, A.; Ickes, J.; et al. Data Products, Quality and Validation of the DLR Earth Sensing Imaging Spectrometer (DESI). *Sensors* **2019**, *19*, 4471, doi:10.3390/s19204471.
 39. Latifi, H.; Holzwarth, S.; Skidmore, A.; Brůna, J.; Červenka, J.; Darvishzadeh, R.; Hais, M.; Heiden, U.; Homolová, L.; Krzystek, P.; et al. A Laboratory for Conceiving Essential Biodiversity Variables (EBVs) – The “Data Pool Initiative for the Bohemian Forest Ecosystem.” *Methods in Ecology and Evolution* **2021**, *12*, 2073–2083, doi:10.1111/2041-210x.13695.
 40. Waldhäuser weather / climate station Available online: <https://www.nationalpark-bayerischerwald.bayern.de/aktuelles/wetterstation/index.htm> (accessed on 7 January 2022).
 41. Abdullah, H.; Darvishzadeh, R.; Skidmore, A.; Heurich, M. Sensitivity of Landsat-8 OLI and TIRS Data to Foliar Properties of Early Stage Bark Beetle (*Ips typographus*, L.) Infestation. *Remote Sensing* **2019**, *11*, 398, doi:10.3390/rs11040398.
 42. Heurich, M.; Beudert, B.; Rall, H.; Křenová, Z. National Parks as Model Regions for Interdisciplinary Long-Term Ecological Research: The Bavarian Forest and Šumavá National Parks Underway to Transboundary Ecosystem Research. In *Long-Term Ecological Research: Between Theory and Application*; 2009; pp. 327–344 ISBN 978-90-481-8781-2.
 43. Christiansen, E.; Bakke, A. The Spruce Bark Beetle of Eurasia. In *Dynamics of Forest Insect Populations: Patterns, Causes, Implications*; Berryman, A.A., Ed.; Population Ecology; Springer US: Boston, MA, 1988; pp. 479–503 ISBN 978-1-4899-0789-9.
 44. Abdullah, H.; Darvishzadeh, R.; Skidmore, A.K.; Heurich, M. Sensitivity of Landsat-8 OLI and TIRS Data to Foliar Properties of Early Stage Bark Beetle (*Ips typographus*, L.) Infestation. *Remote Sensing* **2019**, *11*, 398, doi:10.3390/rs11040398.
 45. Reyes, R.; Langheinrich, M.; Richter, R.; Schwind, P. *Atmospheric Correction in DESIS and EnMAP Processing Chains - An Overview*; 2018;
 46. Hagolle, O.; Huc, M.; Desjardins, C.; Auer, S.; Richter, R. *MAJA Algorithm Theoretical Basis Document*; 2017;
 47. Müller, R.; Avbelj, J.; Carmona, E.; Eckardt, A.; Gerasch, B.; Graham, L.; Günther, B.; Heiden, U.; Ickes, J.; Kerr, G.; et al. THE NEW HYPER SPECTRAL SENSOR DESIS ON THE MULTI-PAYLOAD PLATFORM MUSES INSTALLED ON THE ISS. *ISPRS - International Archives of the Photogrammetry, Remote Sensing and Spatial Information Sciences* **2016**, *XLI-B1*, 461–467, doi:10.5194/isprsarchives-XLI-B1-461-2016.
 48. Sentinel-2 - Satellite Description - Sentinel Online - Sentinel Online Available online: <https://sentinels.copernicus.eu/web/sentinel/missions/sentinel-2/satellite-description> (accessed on 17 February 2022).
 49. Zhu, Z.; Wang, S.; Woodcock, C. Improvement and Expansion of the Fmask Algorithm: Cloud, Cloud Shadow, and Snow Detection for Landsats 4-7, 8, and Sentinel 2 Images. *Remote Sensing of Environment* **2015**, *159*, doi:10.1016/j.rse.2014.12.014.

50. Frantz, D.; Haß, E.; Uhl, A.; Stoffels, J.; Hill, J. Improvement of the Fmask Algorithm for Sentinel-2 Images: Separating Clouds from Bright Surfaces Based on Parallax Effects. *Remote Sensing of Environment* **2018**, *215*, 471–481, doi:10.1016/j.rse.2018.04.046.
51. Rock, B.N.; Hoshizaki, T.; Miller, J.R. Comparison of in Situ and Airborne Spectral Measurements of the Blue Shift Associated with Forest Decline. *Remote Sensing of Environment* **1988**, *24*, 109–127, doi:10.1016/0034-4257(88)90008-9.
52. Beamish, A.L.; Coops, N.; Chabrilat, S.; Heim, B. A Phenological Approach to Spectral Differentiation of Low-Arctic Tundra Vegetation Communities, North Slope, Alaska. *Remote Sensing* **2017**, *9*, 1200, doi:10.3390/rs9111200.
53. de Tomás Marín, S.; Novák, M.; Klančík, K.; Gaberščik, A. Spectral Signatures of Conifer Needles Mainly Depend on Their Physical Traits. *Polish Journal of Ecology* **2016**, *64*, 1–13, doi:10.3161/15052249PJE2016.64.1.001.
54. Zarco-Tejada, P.J.; Hornero, A.; Beck, P.S.A.; Kattenborn, T.; Kempeneers, P.; Hernández-Clemente, R. Chlorophyll Content Estimation in an Open-Canopy Conifer Forest with Sentinel-2A and Hyperspectral Imagery in the Context of Forest Decline. *Remote Sensing of Environment* **2019**, *223*, 320–335, doi:10.1016/j.rse.2019.01.031.
55. Ali, A.; Skidmore, A.; Darvishzadeh, R.; Van Duren, I.; Holzwarth, S.; Müller, J. Retrieval of Forest Leaf Functional Traits from HySpex Imagery Using Radiative Transfer Models and Continuous Wavelet Analysis. *ISPRS Journal of Photogrammetry and Remote Sensing* **2016**, *122*, 68–80, doi:10.1016/j.isprsjprs.2016.09.015.
56. Abdullah, H.; Skidmore, A.; Darvishzadeh, R.; Heurich, M. Sentinel-2 Accurately Maps Green-attack Stage of European Spruce Bark Beetle (*Ips typographus*, L.) Compared with Landsat-8. **2018**, doi:10.1002/rse2.93.
57. Germany's Climate-Stressed Forests Face 'Catastrophe' as Bugs Attack. *The Local Germany* 2019.
58. Morcillo-Pallarés, P.; Rivera-Caicedo, J.P.; Belda, S.; De Grave, C.; Burriel, H.; Moreno, J.; Verrelst, J. Quantifying the Robustness of Vegetation Indices through Global Sensitivity Analysis of Homogeneous and Forest Leaf-Canopy Radiative Transfer Models. *Remote Sensing* **2019**, *11*, 2418, doi:10.3390/rs11202418.
59. Meng, J.; Li, S.; Wang, W.; Liu, Q.; Xie, S.; Ma, W. Mapping Forest Health Using Spectral and Textural Information Extracted from SPOT-5 Satellite Images. *Remote Sensing* **2016**, *8*, 719, doi:10.3390/rs8090719.
60. Huete, A. Vegetation Indices, Remote Sensing and Forest Monitoring. *Geography Compass* **2012**, *6*, doi:10.1111/j.1749-8198.2012.00507.x.
61. Hill, J.; Stoffels, J.; Buddenbaum, H. Die Nutzung des Sentinel-2-Datenarchivs zur zeitnahen Bewertung des Vitalitätszustands von Nadelholzbeständen im Bundesland Rheinland-Pfalz. Folgen des trockenen Spätsommers 2018. 26.
62. Fassnacht, F.; Latifi, H.; Ghosh, A.; Joshi, P.; Koch, B. Assessing the Potential of Hyperspectral Imagery to Map Bark Beetle-Induced Tree Mortality. *Remote Sensing of Environment* **2014**, *140*, 533–548, doi:10.1016/j.rse.2013.09.014.
63. Perkins, R.; Müller, R.; Carmona, E. THE DESIS HYPERSPECTRAL INSTRUMENT – A NEW SPACE-BASED TOOL FOR MONITORING AGRICULTURAL AND WATER RESOURCES. **2017**, *9*.
64. Zarco-Tejada, P.; Miller, J.; Mohammed, G.; Noland, T.; Sampson, P. Vegetation Stress Detection through Chlorophyll + Estimation and Fluorescence Effects on Hyperspectral Imagery. *Journal of environmental quality* **2002**, *31*, 1433–1441, doi:10.2134/jeq2002.1433.
65. Einzmann, K.; Atzberger, C.; Pinnel, N.; Glas, C.; Böck, S.; Seitz, R.; Immitzer, M. Early Detection of Spruce Vitality Loss with Hyperspectral Data: Results of an Experimental Study in Bavaria, Germany. *Remote Sensing of Environment* **2021**, *266*, 112676, doi:10.1016/j.rse.2021.112676.

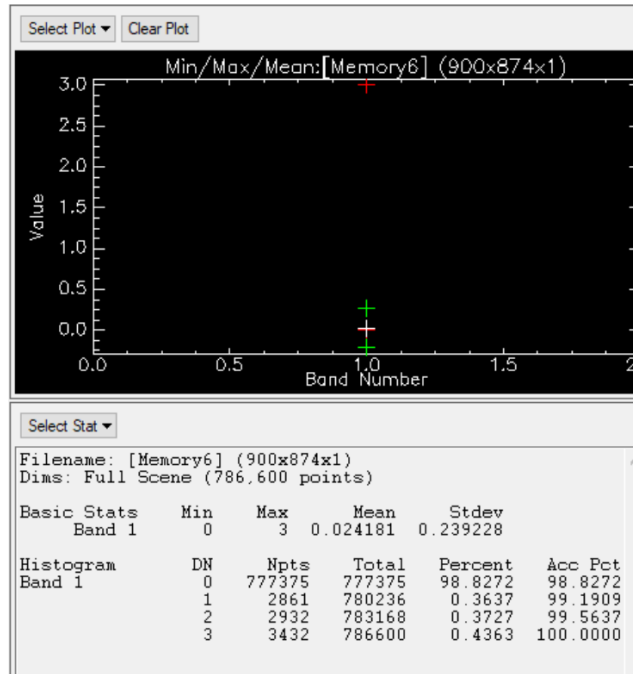
66. Sommer, C.; Holzwarth, S.; Heiden, U.; Heurich, M.; Müller, J.; Mauser, W. FEATURE-BASED TREE SPECIES CLASSIFICATION USING HYPERSPECTRAL AND LIDAR DATA IN THE BAVARIAN FOREST NATIONAL PARK. *EARSeL eProceedings* **2016**, *14*, 49–70, doi:10.12760/02-2015-2-05.
67. Xie, R.; Darvishzadeh, R.; Skidmore, A.K.; Heurich, M.; Holzwarth, S.; Gara, T.W.; Reusen, I. Mapping Leaf Area Index in a Mixed Temperate Forest Using Fenix Airborne Hyperspectral Data and Gaussian Processes Regression. *International Journal of Applied Earth Observation and Geoinformation* **2021**, *95*, 102242, doi:10.1016/j.jag.2020.102242.
68. Merzlyak, M.; Gitelson, A.; Chivkunova, O.; Rakitin, V. Non-destructive Optical Detection of Pigment Changes during Leaf Senescence and Fruit Ripening. **1999**, doi:10.1034/J.1399-3054.1999.106119.X.
69. Peñuelas, J.; Filella, I.; Gamon, J.A. Assessment of Photosynthetic Radiation-Use Efficiency with Spectral Reflectance. *New Phytologist* **1995**, *131*, 291–296, doi:10.1111/j.1469-8137.1995.tb03064.x.
70. Sims, D.A.; Gamon, J.A. Relationships between Leaf Pigment Content and Spectral Reflectance across a Wide Range of Species, Leaf Structures and Developmental Stages. *Remote Sensing of Environment* **2002**, *81*, 337–354, doi:10.1016/S0034-4257(02)00010-X.
71. Datt, B. A New Reflectance Index for Remote Sensing of Chlorophyll Content in Higher Plants: Tests Using Eucalyptus Leaves. *Journal of Plant Physiology* **1999**, *154*, 30–36, doi:10.1016/S0176-1617(99)80314-9.
72. Zarco-Tejada, P.J.; Berjón, A.; López-Lozano, R.; Miller, J.R.; Martín, P.; Cachorro, V.; González, M.R.; de Frutos, A. Assessing Vineyard Condition with Hyperspectral Indices: Leaf and Canopy Reflectance Simulation in a Row-Structured Discontinuous Canopy. *Remote Sensing of Environment* **2005**, *99*, 271–287, doi:10.1016/j.rse.2005.09.002.
73. Datt, B. Remote Sensing of Chlorophyll a, Chlorophyll b, Chlorophyll A+b, and Total Carotenoid Content in Eucalyptus Leaves. *Remote Sensing of Environment* **1998**, *66*, 111–121, doi:10.1016/S0034-4257(98)00046-7.
74. Dotzler, S.; Hill, J.; Buddenbaum, H.; Stoffels, J. The Potential of EnMAP and Sentinel-2 Data for Detecting Drought Stress Phenomena in Deciduous Forest Communities. *Remote Sensing* **2015**, *7*, 14227–14258, doi:10.3390/rs71014227.
75. Gitelson, A.; Merzlyak, M.; Chivkunova, O. Optical Properties and Nondestructive Estimation of Anthocyanin Content in Plant Leaves. *Photochemistry and photobiology* **2001**, *74*, 38–45, doi:10.1562/0031-8655(2001)074<0038:OPANEO>2.0.CO;2.
76. Gitelson, A.; Zur, Y.; Chivkunova, O.; Merzlyak, M. Assessing Carotenoid Content in Plant Leaves with Reflectance Spectroscopy. *Photochemistry and Photobiology* **2002**, *75*, 272–281, doi:10.1562/0031-8655(2002)0750272accipl2.0.co2.
77. VOGELMANN, J.E.; ROCK, B.N.; MOSS, D.M. Red Edge Spectral Measurements from Sugar Maple Leaves. *International Journal of Remote Sensing* **1993**, *14*, 1563–1575, doi:10.1080/01431169308953986.
78. Curran, P.; Windham, W.; Gholz, H. Exploring the Relationship between Reflectance Red Edge and Chlorophyll Concentration in Slash Pine. *Tree physiology* **1995**, *15*, 203–206, doi:10.1093/treephys/15.3.203.
79. Sinergise, S.-H. by Red Edge Position Index (REPO) Available online: https://custom-scripts.sentinel-hub.com/custom-scripts/sentinel-2/red_edge_position/ (accessed on 9 January 2022).
80. Gholizadeh, A.; Mišurec, J.; Kopačková, V.; Mielke, C.; Rogass, C. Assessment of Red-Edge Position Extraction Techniques: A Case Study for Norway Spruce Forests Using HyMap and Simulated Sentinel-2 Data. *Forests* **2016**, *7*, 226, doi:10.3390/f7100226.
81. Daughtry, C.; Walthall, C.; Kim, M.S.; Colstoun, E.B.; McMurtrey, J.E. Estimating Corn Leaf Chlorophyll Concentration from Leaf and Canopy Reflectance. *Remote Sensing of Environment* **2000**, *74*, 229–239, doi:10.1016/S0034-4257(00)00113-9.

82. Barnes, E.; Clarke, T.R.; Richards, S.E.; Colaizzi, P.; Haberland, J.; Kostrzewski, M.; Waller, P.; Choi, C.; Riley, E.; Thompson, T.L. Coincident Detection of Crop Water Stress, Nitrogen Status, and Canopy Density Using Ground Based Multispectral Data. **2000**.
83. Rouse, W.; Haas, R.H. MONITORING VEGETATION SYSTEMS IN THE GREAT PLAINS WITH ERTS. 9.
84. Story, M.; Congalton, R. Accuracy Assessment: A User's Perspective. *undefined* **1986**.
85. Li, S.; Hao, Q.; Gao, G.; Kang, X. The Effect of Ground Truth on Performance Evaluation of Hyperspectral Image Classification. *IEEE Transactions on Geoscience and Remote Sensing* **2018**, *56*, 7195–7206, doi:10.1109/TGRS.2018.2849225.
86. Li, W.; Guo, Q. A New Accuracy Assessment Method for One-Class Remote Sensing Classification. *IEEE Transactions on Geoscience and Remote Sensing* **2014**, *52*, 4621–4632, doi:10.1109/TGRS.2013.2283082.
87. Foody, G. Status of Land Cover Classification Accuracy Assessment. *Remote Sensing of Environment* **2002**, *80*, 185–201, doi:10.1016/S0034-4257(01)00295-4.
88. Su, T.-C. A Filter-Based Post-Processing Technique for Improving Homogeneity of Pixel-Wise Classification Data. *European Journal of Remote Sensing* **2016**, *49*, 531–552, doi:10.5721/EuJRS20164928.
89. Corcoran, J.; Knight, J.; Pelletier, K.; Rampi, L.; Wang, Y. The Effects of Point or Polygon Based Training Data on RandomForest Classification Accuracy of Wetlands. *Remote Sensing* **2015**, *7*, 4002–4025, doi:10.3390/rs70404002.
90. Huo, L.; Persson, H.J.; Lindberg, E. Early Detection of Forest Stress from European Spruce Bark Beetle Attack, and a New Vegetation Index: Normalized Distance Red & SWIR (NDRS). *Remote Sensing of Environment* **2021**, *255*, 112240, doi:10.1016/j.rse.2020.112240.
91. Wong, C.; Gamon, J. Three Causes of Variation in the Photochemical Reflectance Index (PRI) in Evergreen Conifers. *New Phytologist* **2014**, *206*, doi:10.1111/nph.13159.
92. Wong, C.Y.S.; D'Odorico, P.; Bhatena, Y.; Arain, M.A.; Ensminger, I. Carotenoid Based Vegetation Indices for Accurate Monitoring of the Phenology of Photosynthesis at the Leaf-Scale in Deciduous and Evergreen Trees. *Remote Sensing of Environment* **2019**, *233*, 111407, doi:10.1016/j.rse.2019.111407.
93. Haboudane, D.; Miller, J.R.; Pattey, E.; Zarco-Tejada, P.J.; Strachan, I.B. Hyperspectral Vegetation Indices and Novel Algorithms for Predicting Green LAI of Crop Canopies: Modeling and Validation in the Context of Precision Agriculture. *Remote Sensing of Environment* **2004**, *90*, 337–352, doi:10.1016/j.rse.2003.12.013.
94. Modzelewska, A.; Stereńczak, K.; Mierczyk, M.; Maciuk, S.; Balazy, R.; Zawila-Niedźwiecki, T. Sensitivity of Vegetation Indices in Relation to Parameters of Norway Spruce Stands. *Folia Forestalia Polonica* **2017**, *59*, doi:10.1515/ffp-2017-0009.
95. Nink, S.; Hill, J.; Stoffels, J.; Buddenbaum, H.; Frantz, D.; Langshausen, J. Using Landsat and Sentinel-2 Data for the Generation of Continuously Updated Forest Type Information Layers in a Cross-Border Region. *Remote Sensing* **2019**, *11*, 2337, doi:10.3390/rs11202337.
96. Ortiz-Rivera, V.; Velez-Reyes, M.; Roysam, B. *Change Detection in Hyperspectral Imagery Using Temporal Principal Components*; 2006;

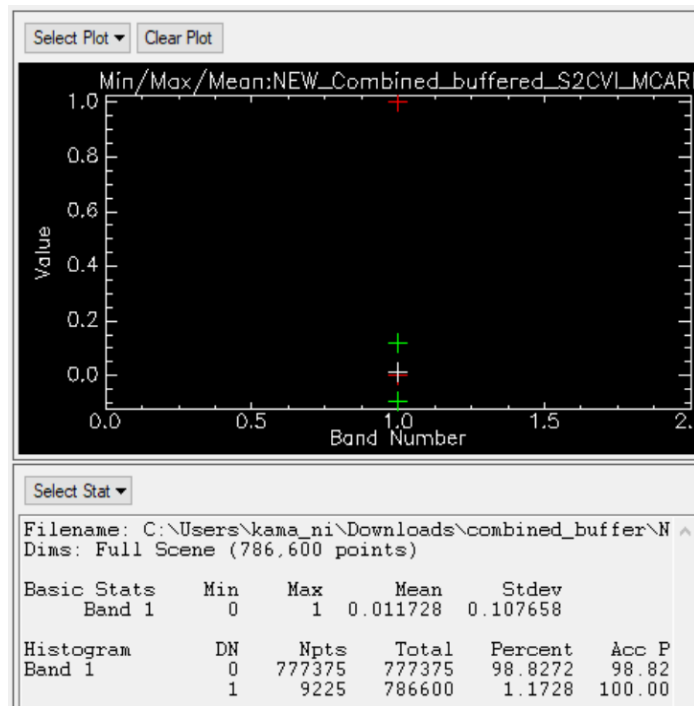
APPENDICES

Appendix 1: Combined Detection Index

Statistics for modified Combined detection index "2*MCARI + CVI"

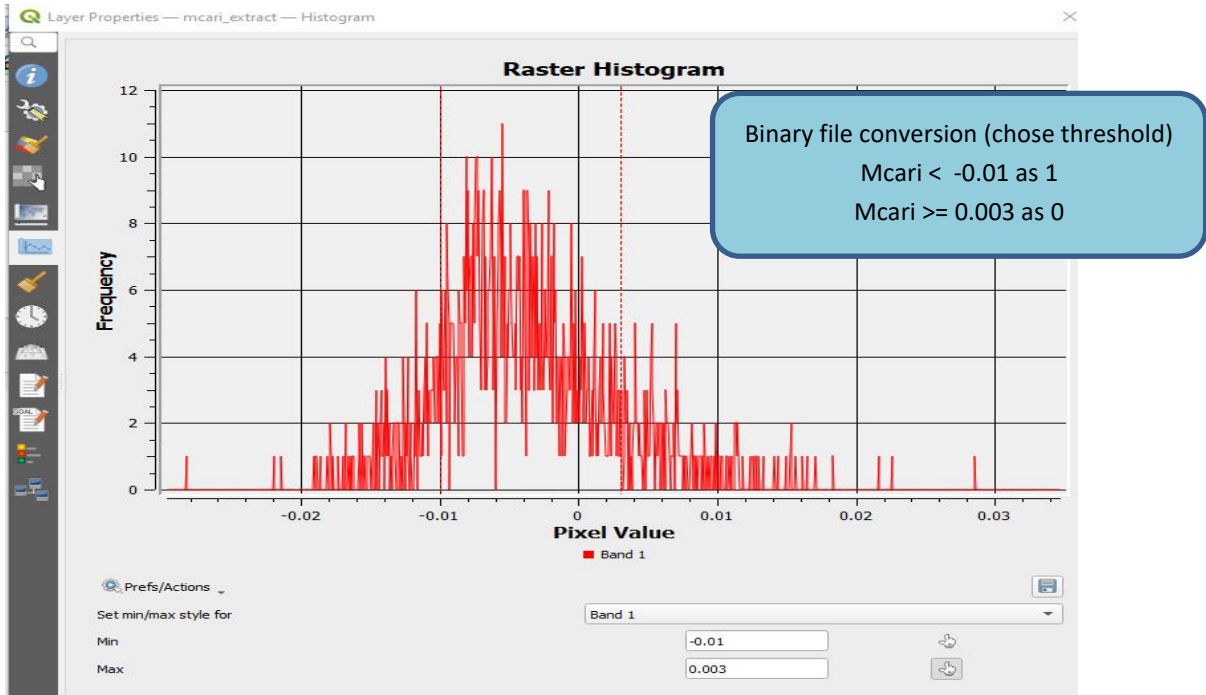


Combined detection index to binary – Changes detected by DESIS + S2 + both



Appendix 2: Accuracy assessment

MCARI Threshold definition



MCARI Original derived Accuracy - Correct No change 84% and Correct change 18%

Class Confusion Matrix

Confusion Matrix: [Memory1] (900x874x1)

Overall Accuracy = (2829/3491) 81.0370%
 Kappa Coefficient = 0.0175

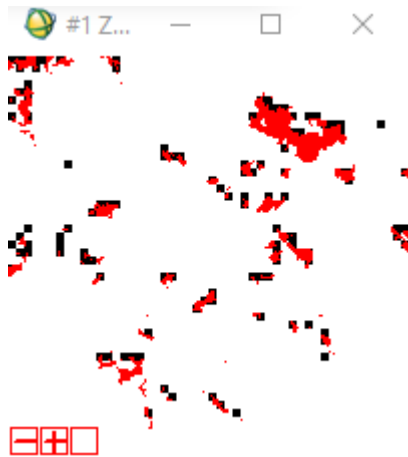
Class	Ground Truth (Pixels)		Total
	Unclassified	EVF: Layer: d	
Unclassified	2792	167	2959
Class #1	495	37	532
Total	3287	204	3491

Class	Ground Truth (Percent)		Total
	Unclassified	EVF: Layer: d	
Unclassified	84.94	81.86	84.76
Class #1	15.06	18.14	15.24
Total	100.00	100.00	100.00

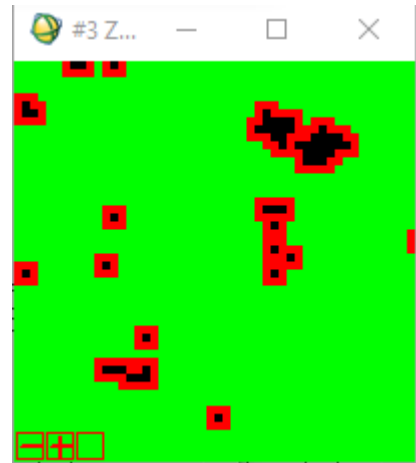
Class	Commission (Percent)	Omission (Percent)	Commission (Pixels)	Omission (Pixels)
	Unclassified	5.64	15.06	167/2959
Class #1	93.05	81.86	495/532	167/204

Class	Prod. Acc. (Percent)	User Acc. (Percent)	Prod. Acc. (Pixels)	User Acc. (Pixels)
	Unclassified	84.94	94.36	2792/3287
Class #1	18.14	6.95	37/204	37/532

MCARI Buffer to 30 meters



(a)



(b)

a) MCARI binary image overlaid with ground truth ROI in change regions

b) Buffer for "change class" to 30 meters (identified change regions)

MCARI One pixel buffer accuracy - Correct No change 65% and Correct change 79%

Class Confusion Matrix

File

Confusion Matrix: [Memory3] (900x874x1)

Overall Accuracy = (4185/6364) 65.7605%

Kappa Coefficient = 0.0688

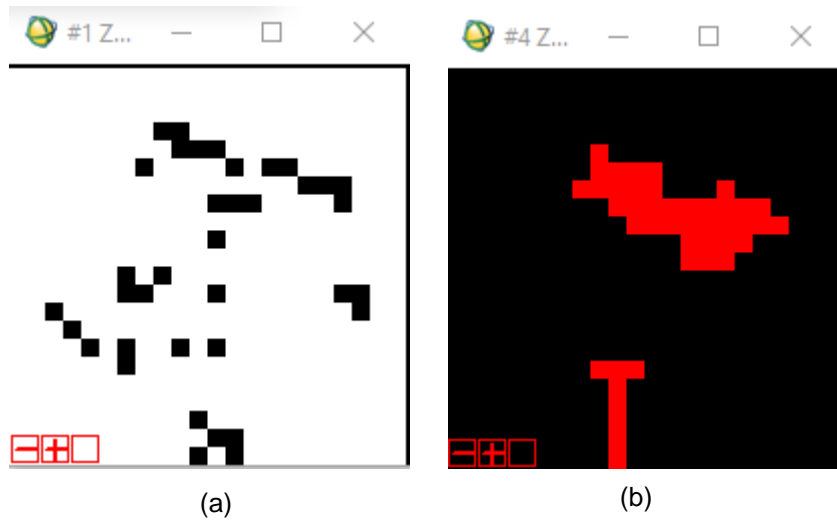
Class	Ground Truth (Pixels)		Total
	Unclassified	EVF: Layer: d	
Unclassified	4038	38	4076
Class #1	2141	147	2288
Total	6179	185	6364

Class	Ground Truth (Percent)		Total
	Unclassified	EVF: Layer: d	
Unclassified	65.35	20.54	64.05
Class #1	34.65	79.46	35.95
Total	100.00	100.00	100.00

Class	Commission (Percent)	Omission (Percent)	Commission (Pixels)	Omission (Pixels)
	Unclassified	0.93	34.65	38/4076
Class #1	93.58	20.54	2141/2288	38/185

Class	Prod. Acc. (Percent)	User Acc. (Percent)	Prod. Acc. (Pixels)	User Acc. (Pixels)
	Unclassified	65.35	99.07	4038/6179
Class #1	79.46	6.42	147/185	147/2288

MCARI Clump class



a) MCARI binary image

b) Clump class for "Change class" only (identified change regions)

MCARI Clump class accuracy - Correct No change 68% and Correct change 70%

Class Confusion Matrix

File

Confusion Matrix: [Memory5] (900x874x1)

Overall Accuracy = (4435/6428) 68.9950%

Kappa Coefficient = 0.0664

Class	Ground Truth (Pixels)		Total
	Unclassified	EVF: Layer: d	
Unclassified	4304	56	4360
Class #1	1937	131	2068
Total	6241	187	6428

Class	Ground Truth (Percent)		Total
	Unclassified	EVF: Layer: d	
Unclassified	68.96	29.95	67.83
Class #1	31.04	70.05	32.17
Total	100.00	100.00	100.00

Class	Commission (Percent)	Omission (Percent)	Commission (Pixels)	Omission (Pixels)
	Unclassified	1.28	31.04	56/4360
Class #1	93.67	29.95	1937/2068	56/187

Class	Prod. Acc. (Percent)	User Acc. (Percent)	Prod. Acc. (Pixels)	User Acc. (Pixels)
	Unclassified	68.96	98.72	4304/6241
Class #1	70.05	6.33	131/187	131/2068

In a similar way, accuracy estimated for S2 CVI

CVI Original accuracy - Correct No change 84% and Correct change 20%

Class Confusion Matrix

File

Confusion Matrix: [Memory1] (1350x1399x1)
 Overall Accuracy = (1297/6264) 20.7056%
 Kappa Coefficient = 0.0004

Class		Ground Truth (Pixels)		Total
Unclassified	Class #1	Unclassified	Class #1	
Unclassified		16	4964	4980
Class #1		3	1281	1284
Total		19	6245	6264

Class		Ground Truth (Percent)		Total
Unclassified	Class #1	Unclassified	Class #1	
Unclassified		84.21	79.49	79.50
Class #1		15.79	20.51	20.50
Total		100.00	100.00	100.00

Class		Commission (Percent)	Omission (Percent)	Commission (Pixels)	Omission (Pixels)
Unclassified		99.68	15.79	4964/4980	3/19
Class #1		0.23	79.49	3/1284	4964/6245

Class		Prod. Acc. (Percent)	User Acc. (Percent)	Prod. Acc. (Pixels)	User Acc. (Pixels)
Unclassified		84.21	0.32	16/19	16/4980
Class #1		20.51	99.77	1281/6245	1281/1284

CVI Buffer pixels accuracy - Correct No change 52% and Correct change 61%

Class Confusion Matrix

File

Confusion Matrix: [Memory4] (1350x1399x1)
 Overall Accuracy = (7556/13830) 54.6349%
 Kappa Coefficient = 0.1019

Class		Ground Truth (Pixels)		Total
Unclassified	Class #1	Unclassified	Class #1	
Unclassified		5493	1284	6777
Class #1		4990	2063	7053
Total		10483	3347	13830

Class		Ground Truth (Percent)		Total
Unclassified	Class #1	Unclassified	Class #1	
Unclassified		52.40	38.36	49.00
Class #1		47.60	61.64	51.00
Total		100.00	100.00	100.00

Class		Commission (Percent)	Omission (Percent)	Commission (Pixels)	Omission (Pixels)
Unclassified		18.95	47.60	1284/6777	4990/10483
Class #1		70.75	38.36	4990/7053	1284/3347

Class		Prod. Acc. (Percent)	User Acc. (Percent)	Prod. Acc. (Pixels)	User Acc. (Pixels)
Unclassified		52.40	81.05	5493/10483	5493/6777
Class #1		61.64	29.25	2063/3347	2063/7053

CVI Clump class accuracy - Correct No change 71% and Correct change 86%

Class Confusion Matrix

File

Confusion Matrix: [Memory6] (1350x1399x1)
 Overall Accuracy = (10539/14026) 75.1390%
 Kappa Coefficient = 0.4635

Class		Ground Truth (Pixels)		Total
Unclassified	Class #1	Unclassified	Class #1	
Unclassified		7564	455	8019
Class #1		3032	2975	6007
Total		10596	3430	14026

Class		Ground Truth (Percent)		Total
Unclassified	Class #1	Unclassified	Class #1	
Unclassified		71.39	13.27	57.17
Class #1		28.61	86.73	42.83
Total		100.00	100.00	100.00

Class		Commission (Percent)	Omission (Percent)	Commission (Pixels)	Omission (Pixels)
Unclassified		5.67	28.61	455/8019	3032/10596
Class #1		50.47	13.27	3032/6007	455/3430

Class		Prod. Acc. (Percent)	User Acc. (Percent)	Prod. Acc. (Pixels)	User Acc. (Pixels)
Unclassified		71.39	94.33	7564/10596	7564/8019
Class #1		86.73	49.53	2975/3430	2975/6007